

# Stable isotopic evidence for Neogene surface downdrop in the central Basin and Range Province

Travis W. Horton<sup>†</sup>

Geology Department, University of Puget Sound, Tacoma, Washington 98416-1048, USA

C. Page Chamberlain

Department of Geological and Environmental Sciences, Stanford University, Stanford, California 94305-2115, USA

## ABSTRACT

**Authigenic calcite and smectite stable isotope records were determined for five Neogene terrestrial stratigraphic sections from the central Basin and Range Province and surrounding regions. We recognized a general pattern of increasing authigenic mineral  $\delta^{18}\text{O}$  values with decreasing age since the middle Miocene throughout the region. We suggest this pattern results from regional elevation decrease and associated changes in atmospheric circulation patterns. An anomalous pattern of decreasing  $\delta^{18}\text{O}$  values with decreasing age is observed in the Miocene Horse Spring Formation exposed in the Lake Mead Basin, which is contemporaneous with local magmatic activity. We suggest this pattern results from surficial uplift of local highlands feeding water into the Horse Spring depositional system. The topographic histories suggested here provide insight into the response of the land surface to crustal processes. Neogene extensional deformation in the central Basin and Range Province resulted in a net regional elevation decrease.**

**Keywords:** isotope ratios, lacustrine sediments, Basin and Range Province, paleotopography, Neogene.

## INTRODUCTION

Determining the topographic response of elevated regions to changes in lithospheric structure is an important yet poorly understood problem in the earth sciences. The surface uplift of mountain belts, such as the Himalaya and Andes, is generally agreed to result from the development of a thick (70–80 km) Airy-type

crustal root during collisional tectonic events (Wernicke et al., 1996). In contrast, loss of a preexisting Airy-type crustal root is believed to have occurred during the late Cenozoic beneath the Sierra Nevada range of California (Wernicke et al., 1996). The topographic response to this change in crustal structure is debated in the scientific literature, thus complicating our ability to interpret the long-term linkages between topography and climate in the region (e.g., Wernicke et al., 1996; Farmer et al., 2002; Jones et al., 2004).

Several recent investigations provide insight into the lithospheric structure of the southern Sierra Nevada and adjacent central Basin and Range Province region (e.g., Wernicke et al., 1996; Rudnick and Lee, 2002). One of the most intriguing contributions from these studies is the observation that the Sierra Nevada and adjacent Basin and Range Province are underlain by continental crust of similar thickness (Wernicke et al., 1996). This discovery is surprising in that the southern Sierra Nevada stands ~1.8–2.8 km above the central Basin and Range Province east of the range, suggesting the Sierra Nevada is supported by low-density upper mantle (Ducea and Saleeby, 1998). Compelling petrologic, geophysical, and geochemical evidence exists for the removal of a preexisting crustal root beneath the southern Sierra Nevada, and replacement of this deep crust by asthenosphere since the middle Miocene (Fliedner and Ruppert, 1996; Ducea and Saleeby, 1998; Farmer et al., 2002; Rudnick and Lee, 2002; Jones et al., 2004).

Despite these advances, the topographic response to changes in lithospheric structure across the southern Sierra Nevada–central Basin and Range transition is not well known. Some studies have suggested that upwelling of low-density asthenosphere beneath the Sierra Nevada resulted in significant topographic uplift of the range during the late Neogene (e.g., Ruppert et al., 1998; Farmer et al., 2002). In contrast, others

have suggested that negative buoyancy forces could have caused up to 4 km of topographic lowering of the range during this same period of time (Wernicke et al., 1996). Results from paleotopographic investigations of the Sierra Nevada and adjacent Basin and Range have produced similarly disparate interpretations of the uplift history of the region.

Paleotopographic arguments supporting post–middle Miocene uplift of the Sierra Nevada are based on geomorphic (e.g., Christensen, 1966; Huber, 1981) and paleofloral (e.g., Axelrod, 1962) data sets, whereas paleotopographic arguments supporting pre–middle Miocene uplift of the range are based on paleofloral (Wolfe et al., 1997), thermochronologic (House et al., 1998), and stable isotopic (Poage and Chamberlain, 2002) data sets. One of the most significant results of Poage and Chamberlain's study (2002) is the identification of an ~5‰ increase in smectite and calcite  $\delta^{18}\text{O}$  values between 14 and 7 Ma for samples collected from the El Paso Basin, ~30 km east of the southern Sierra Nevada range crest. A similar age and magnitude isotopic shift is not recognized in other terrestrial basin stable isotopic records produced throughout the northern Basin and Range Province (Poage and Chamberlain, 2002; Horton et al., 2004). Poage and Chamberlain (2002) suggested that the increase in smectite and calcite  $\delta^{18}\text{O}$  values in the El Paso Basin records a localized shift in surface-water  $\delta^{18}\text{O}$  values, possibly caused by a 2 km reduction in surface elevation of the southern Sierra or changes in regional storm tracks that circumnavigate the southern Sierra en route to the El Paso Basin. To test these hypotheses, we examined five additional Neogene authigenic mineral stable isotopic records from the central Basin and Range Province and California Transverse Range in an effort to better constrain regional versus local patterns in stable isotopic stratigraphic records.

<sup>†</sup>E-mail: thorton@ups.edu.

All of the authigenic mineral stable isotopic records presented here exhibit isotopic shifts toward more positive  $\delta^{18}\text{O}$  values with decreasing age since the middle Miocene. However, none of the isotopic records presented here matches the precise age and magnitude of the isotopic shift observed in the El Paso Basin record of Poage and Chamberlain (2002). We suggest that a regional surface elevation decrease, and associated reorganization of regional climate patterns, is responsible for the observed increase in authigenic mineral  $\delta^{18}\text{O}$  values with decreasing age throughout the central Basin and Range.

In addition, the Neogene calcite oxygen isotope record produced for the Lake Mead Basin shows an early to middle Miocene decrease in  $\delta^{18}\text{O}$  values that is not recognized in any of the other stratigraphic sections investigated. We suggest the anomalous patterns recognized in the El Paso Basin and Lake Mead Basin stable isotopic records result from local surface subsidence and uplift events, respectively. Topographic lowering of the El Paso Basin during the middle to late Miocene agrees well with documented changes in sediment provenance during this time (Loomis and Burbank, 1988). Uplift in

the Lake Mead area during the Miocene is also supported by sedimentologic reconstructions of regional paleogeography (Beard, 1996).

### GEOLOGIC SETTING

The stratigraphic sections investigated in the current study, including sedimentary sequences exposed in the San Gabriel Mountains (Soledad Basin), Mud Hills (Rainbow Basin), Cottonwood and Funeral Mountains (Death Valley area), Virgin Mountains (Lake Mead Basin), and Artillery Mountains (western Arizona), are spread across an  $\sim 100,000$  km<sup>2</sup> area of the central Basin and Range Province and surrounding areas (Fig. 1). These sedimentary sections were all deposited in extensional rift basins characteristic of the central Basin and Range Province during the Neogene. Detailed lithostratigraphic descriptions of the sedimentary rocks investigated are provided in the following sources: Soledad Basin (Muehlberger, 1958; Ehlert, 1982; Hendrix and Ingersoll, 1987); Rainbow Basin (MacFadden et al., 1990; Woodburne et al., 1990; Ingersoll et al., 1996); Death Valley region (Blair and Reynolds, 1999; Cemen et al.,

1999; Snow and Lux, 1999); Lake Mead area (Bohannon, 1984; Beard, 1996); and western Arizona (Sheppard and Gude, 1973; Spencer et al., 1989). For each of the stratigraphic sections investigated, a brief summary description is presented next.

The Soledad Basin includes 8000 m of fluvio-lacustrine sedimentary rocks ranging in age from 25 to 2 Ma (Durham et al., 1954; Crowell, 1973; Hendrix and Ingersoll, 1987), and lies west of the central Basin and Range, where most of our sections are located. The depositional basin originally formed in response to northwest-southeast-oriented crustal extension, possibly related to northward migration of the Mendocino triple junction (Hendrix and Ingersoll, 1987). Paleogeographic reconstructions indicate the Soledad Basin was originally located adjacent to the ancestral San Gabriel Mountains, near the present-day Salton Sea (Hendrix and Ingersoll, 1987). The lower 6000 m of Soledad Basin fill is assigned to the early Miocene (25–21 Ma) Vasquez Formation (Hendrix and Ingersoll, 1987). Samples from the Vasquez Formation investigated in the current study were collected from lacustrine sediments of the Volcanic–Tick Canyon interval of the lower Vasquez Formation (Hendrix and Ingersoll, 1987). The middle and upper Miocene Tick Canyon and Mint Canyon Formations unconformably overlie the Vasquez Formation in the Soledad Basin stratigraphic section (Hendrix and Ingersoll, 1987). No samples were investigated from the  $\sim 200$ -m-thick Tick Canyon Formation in the current study. Samples from the Mint Canyon Formation investigated in the current study were collected from Area D of Ehlert (1982). These samples include calcareous lacustrine mudstones and algal limestones collected from an  $\sim 1000$ -m-thick sequence of lacustrine sedimentary rocks west of Bouquet Canyon. Additional lacustrine limestone samples were collected from the  $\sim 400$ -m-thick upper Pliocene Sunshine Ranch Member of the Saugus Formation (Morrison, 1965).

Rainbow Basin, in the southern Mud Hills  $\sim 10$  km north of Barstow, California, includes  $\sim 1000$  m of fluvio-lacustrine sedimentary rocks of the middle Miocene Barstow Formation (Ingersoll et al., 1996). The Barstow Formation represents postextensional basin fill, including coarse- to fine-grained sedimentary rocks and water-laid volcanic ash (MacFadden et al., 1990). Several radiometric age determinations on tuffs exposed throughout the Barstow Formation constrain the age of deposition between ca. 20 and ca. 13 Ma (MacFadden et al., 1990; Woodburne et al., 1990). Samples investigated in the current study included smectitic ashes, calcareous mudstones, and lacustrine limestones exposed throughout the Barstow Formation. In

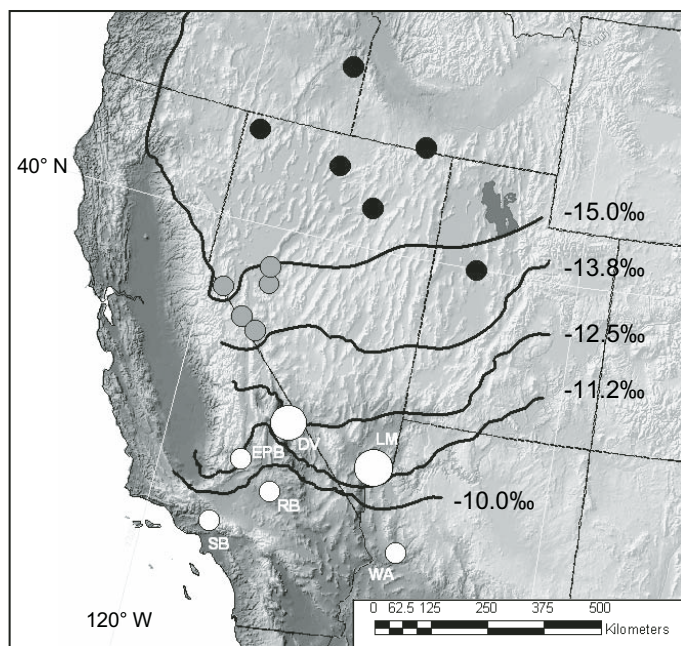


**Figure 1.** Digital elevation model of the southwestern United States with stratigraphic section locations. Stratigraphic sections from the northern Great Basin (Horton et al., 2004) are shown as black circles. Stratigraphic sections from the western Great Basin (Poage and Chamberlain, 2002) are shown as gray circles. Stratigraphic sections investigated in the current study and the El Paso Basin of Poage and Chamberlain (2002) are shown as white circles. These sections include: SB—Soledad Basin; EPB—El Paso Basin; RB—Rainbow Basin; DV—Death Valley area; LM—Lake Mead area; WA—western Arizona. Also shown are  $\delta^{18}\text{O}$  contours of modern precipitation throughout the Great Basin region (Friedman et al., 2002b).

addition, two smectitic ash layers from the Pliocene Mojave River Formation of Nagy and Murray (1996), exposed ~50 km east of Barstow, were included in the current investigation.

Detailed lithostratigraphic descriptions of the Neogene terrestrial sedimentary rocks exposed in the Death Valley region are available in the literature (e.g., Blair and Reynolds, 1999; Cemen et al., 1999; Snow and Lux, 1999; Wright et al., 1999). For the current study, samples were collected from the lower Miocene Ubehebe, middle Miocene Panuga and Bat Mountain, and the upper Miocene Furnace Creek Formations. The lower Miocene Ubehebe and middle Miocene Panuga and Bat Mountain Formations represent early and synextensional basin-fill sequences of both coarse-grained lithic facies and lacustrine facies (Cemen et al., 1999; Snow and Lux, 1999). Only samples of lacustrine limestone and marl were collected for the current investigation. Radiometric ages determined for volcanic ashes included in the Ubehebe Formation constrain the age of deposition between ca. 25 and ca. 20 Ma (Snow and Lux, 1999), and ca. 15.7 Ma for the Panuga Formation (Snow and Lux, 1999). The overlying ~2000-m-thick Furnace Creek Formation was deposited between ca. 4 and ca. 7 Ma, during a period of rapid subsidence following significant crustal extension in the Death Valley region (Cemen et al., 1999; Wright et al., 1999). Lacustrine mudstones, limestone, and water-laid tuffs, locally including evaporite minerals (e.g., borates and gypsum), characterize the Furnace Creek Formation (Wright et al., 1999). Calcite-bearing mudstones and limestones were sampled exclusively for the current investigation.

Terrestrial sedimentary rocks in the Lake Mead area include the Miocene Horse Spring and Muddy Creek Formations (Bohannon, 1984). Lacustrine limestones and calcareous shales of the Horse Spring Formation were collected east of Frenchman Mountain, near Las Vegas, Nevada, in the current investigation. These samples range in age from ca. 26 (Beard, 1996) to ca. 12 Ma (Bohannon, 1984) based on several radiometric age determinations. Additional lacustrine limestones and calcareous shales were collected from the overlying Muddy Creek Formation of late Miocene age (Anderson et al., 1972; Bohannon, 1984). The Neogene terrestrial sedimentary rocks of the Lake Mead region include pre- and synextensional lacustrine facies with interbedded fluvial deposits (Bohannon, 1984; Beard, 1996). The Neogene stratigraphic section in the Lake Mead area is of particular significance to the current investigation because it is the only stratigraphic sequence investigated that includes pre-extensional sedimentary units, specifically the Rain-

bow Gardens Member of the Horse Spring Formation. The Rainbow Gardens Member is an ~200-m-thick sequence of lacustrine limestones and fluvial sandstones that range in age between ca. 26 and ca. 19 Ma (Beard, 1996). Basin analysis of the Rainbow Gardens Member suggests the unit was deposited in a low-lying shallow lake basin south of the Sevier thrust belt highlands, contemporaneous with regional magmatism related to the Great Basin "ignimbrite flareup" (Beard, 1996).

Nonmarine sedimentary rocks in western Arizona include the Artillery, Chapin Wash, and Big Sandy Formations of Miocene through Pliocene age (Nations et al., 1982). The ~2000-m-thick Artillery Formation is divided into lower (~700 m), middle (~1000 m), and upper (~300 m) members consisting of conglomeratic sandstone, mudstone, and limestone (lower member), sedimentary breccia, conglomerate, and basalt (middle member), and megabreccia (upper member), respectively (Spencer et al., 1989). The overlying Chapin Wash Formation is an ~300-m-thick sandstone unit. Radiometric ages determined for volcanic rocks within and immediately overlying the Artillery and Chapin Wash Formations indicate these units were deposited between ca. 23 and ca. 10 Ma (Shafiqullah et al., 1980; Spencer et al., 1989). The Pliocene Big Sandy Formation is exposed ~40 km north of the Artillery Mountains near Wikieup, Arizona. The Big Sandy Formation is an ~75-m-thick sequence of lacustrine mudstone and zeolite altered tuffs (Sheppard and Gude, 1973). For the current investigation, only samples from the calcite-bearing lacustrine units of the lower member of the Artillery and Big Sandy Formations were collected.

## METHODS

### Carbonate Stable Isotope Analyses

Carbonate oxygen and carbon isotope analyses were performed in the Stable Isotope Biogeochemistry Laboratory at Stanford University using a modified version of the technique described by McCrea (1950). Approximately 1–2 mg of carbonate powder was extracted from lacustrine limestone and calcareous shale samples using a dentist's drill and then reacted at 70 °C with pure phosphoric acid in sealed reaction vessels flushed with helium gas. Headspace sampling of evolved CO<sub>2</sub> was performed with a Finnigan Gas-Bench, and isotopic ratios were measured on a Finnigan Delta+XL mass spectrometer. Precision of the carbonate isotopic data is ~0.2‰ for both oxygen and carbon isotope ratios, based on blind duplicate analysis of NBS-18 and NBS-19 carbonate standards.

### Smectite Stable Isotope Analyses

Clay-size mineral separates were extracted from air-fall ash deposits using standard centrifugation methods (Moore and Reynolds, 1997). Clay-water slurries were then mounted on glass slides and allowed to dry overnight for subsequent X-ray diffraction analysis on a Rigaku X-Ray diffractometer. Oriented samples were X-rayed to determine constituent clay mineralogy. Only samples of pure smectite were used for oxygen and hydrogen isotope analysis.

Oxygen isotope ratios of smectite separates were determined using methods modified from Clayton and Mayeda (1963). From 10 to 15 mg of smectite separate was placed in a N-atmosphere drybox overnight in the presence of P<sub>2</sub>O<sub>5</sub> before loading into nickel reaction vessels. Reaction vessels were evacuated, heated to ~200 °C for 1 h, and reevacuated before reaction with BrF<sub>3</sub> at 570 °C for 16 h. Oxygen generated from this reaction was reacted with a heated graphite rod to produce CO<sub>2</sub>. Generated CO<sub>2</sub> was purified cryogenically and injected directly into a Finnigan Delta+XL mass spectrometer for oxygen isotope ratio determinations. Precision of the determined smectite oxygen isotope ratios is ~0.2‰, based on repeated analysis of internal laboratory smectite standard DS15.

Smectite hydrogen isotope ratios were determined using the method of Sharp et al. (2001). From 0.5 to 1 mg of smectite separate wrapped in a silver foil capsule was dropped into a Finnigan high-temperature conversion elemental analyzer (TC-EA) using an autosampler. Wrapped samples reacted in the TC-EA furnace at 1450 °C in a helium stream generating H<sub>2</sub> gas. The evolved gas passed through a 5 Å molecular sieve gas chromatography column and was introduced via a Finnigan ConFlo III interface to a Finnigan Delta+XL mass spectrometer for hydrogen isotope ratio determinations under continuous-flow conditions. Precision of the determined smectite hydrogen isotope ratios is ±2.5‰, based on repeated analysis of NBS standards 22 and 30.

### Carbonate Trace Element Analyses

Carbonate Mg/Ca and Sr/Ca ratios were determined using a sensitive high-resolution ion microprobe (SHRIMP)-Reverse Geometry at Stanford University using the method of Meibom et al. (2003). An ~10 KeV primary beam of O<sup>2+</sup> ions was focused to a diameter of ~25 μm on the surface of epoxy mounted carbonate grains. Sputtered secondary ion (<sup>43</sup>Ca<sup>2+</sup>, <sup>88</sup>Sr<sup>2+</sup> and <sup>24</sup>Mg<sup>2+</sup>) peak intensities were measured in an electron multiplier following magnetic sector and electrostatic analyzer secondary beam focusing. Elemental ratios were

determined using working curves for  $^{88}\text{Sr}/^{43}\text{Ca}$  and  $^{24}\text{Mg}/^{43}\text{Ca}$  intensity ratios against Sr/Ca and Mg/Ca ratios of a series of internal laboratory calcite standards of known composition. The elemental ratios reported are precise to  $\pm 0.5\%$ , based on repeated analysis of the standard material. Internal laboratory calcite standards were synthesized from mixtures of Spec-pure  $\text{CaCO}_3$ , with varying amounts of Sr and Mg spikes, in a piston-cylinder apparatus by Ben Hankins and John Fitzpatrick at the U.S. Geological Survey (USGS) in Menlo Park, California (Meibom et al., 2003). Calcite standard elemental concentrations were determined at the USGS by solution inductively coupled plasma-mass spectrometry (ICP-MS) and checked for homogeneity with the SHRIMP-RG.

### STABLE ISOTOPIC RESULTS

In total, we determined the  $\delta^{18}\text{O}$  and  $\delta^{13}\text{C}$  values of 199 lacustrine carbonates from the Neogene terrestrial basins (Table 1). The carbonates from the Soledad Basin range from  $-5.5\%$  to  $-14.2\%$   $\delta^{18}\text{O}$  (Peedee belemnite [PDB]) and from  $-5.3\%$  to  $-13.8\%$  for  $\delta^{13}\text{C}$  (PDB); the lacustrine carbonates from the Rainbow Basin range from  $-6.0\%$  to  $-9.1\%$   $\delta^{18}\text{O}$  (PDB) and from  $1.1\%$  to  $-4.3\%$  for  $\delta^{13}\text{C}$  (PDB); the carbonates from the Death Valley region range from  $-5.0\%$  to  $-16.5\%$   $\delta^{18}\text{O}$  (PDB) and from  $4.7\%$  to  $-5.7\%$  for  $\delta^{13}\text{C}$  (PDB); the lacustrine carbonates from the Lake Mead Basin range from  $-1.1\%$  to  $-14.1\%$   $\delta^{18}\text{O}$  (PDB) and from  $10.8\%$  to  $-4.3\%$  for  $\delta^{13}\text{C}$  (PDB); and the lacustrine carbonates from western Arizona range from  $-5.0\%$  to  $-10.7\%$   $\delta^{18}\text{O}$  (PDB) and from  $2.5\%$  to  $-5.0\%$  for  $\delta^{13}\text{C}$  (PDB).

We also measured the smectite  $\delta^{18}\text{O}$  and  $\delta\text{D}$  values for 10 samples from air-fall ashes collected from the El Paso Basin and Rainbow Basin stratigraphic sections (Table 2). Smectite  $\delta^{18}\text{O}$  values range from  $21.0\%$  to  $13.6\%$  (standard mean ocean water [SMOW]) and  $\delta\text{D}$  values range from  $-102\%$  to  $-111\%$  (SMOW) in the El Paso Basin, and smectite  $\delta^{18}\text{O}$  values range from  $19.2\%$  to  $15.6\%$  (SMOW) and  $\delta\text{D}$  values range from  $-96\%$  to  $-110\%$  (SMOW) in the Rainbow Basin.

Lacustrine carbonate  $\delta^{18}\text{O}$  values are plotted against age in Figure 2. Sample ages were assigned based on published radiometric ages (see previous section for age data and references) and stratigraphic position relative to dated samples assuming a linear accumulation rate. For the Lake Mead Basin (Fig. 2D), individual sample ages were not assigned due to the limited occurrence of datable materials in the stratigraphic intervals sampled. As such, lacustrine carbonate  $\delta^{18}\text{O}$  values for Lake Mead

Basin samples are presented as whiskered quartile boxes spanning the published age range for the lithostratigraphic units indicated (Fig. 2D). Whiskers extending from each quartile box in Figure 2D span the upper and lower quartiles for the  $\delta^{18}\text{O}$  data presented in Table 1 for the lithostratigraphic unit indicated. The median  $\delta^{18}\text{O}$  value for lacustrine carbonates analyzed for each unit is represented by the vertical hachure inside each quartile box (Fig. 2D). The total number ( $n$ ) of samples analyzed from each unit is also indicated (Fig. 2D). Carbonate  $\delta^{18}\text{O}$  values for the Miocene-Pliocene Bouse Formation, determined by Poulson and John (2003), are presented in similar style (Fig. 2D). Authigenic mineral stable isotopic records from previously published investigations in the northern (Horton et al., 2004) and western (Poage and Chamberlain, 2002) Great Basin, and El Paso Basin (Poage and Chamberlain 2002) are presented for comparison (Fig. 2F).

These stable isotopic data show the following: First, all of the stable isotopic records show an overall increasing trend in authigenic calcite  $\delta^{18}\text{O}$  values with decreasing age since the middle Miocene (Fig. 2A–E). This general pattern is similar to previously published stable isotopic records for other Neogene stratigraphic sequences exposed elsewhere in the Great Basin region (Poage and Chamberlain, 2002; Horton et al., 2004; Fig. 2F). The absolute magnitude of the Miocene increases in calcite  $\delta^{18}\text{O}$  values recognized in the Soledad Basin, Rainbow Basin, Death Valley area, Lake Mead region, and western Arizona isotope stratigraphies varies from a maximum of  $\sim 8\%$  in the Death Valley area to a minimum of  $\sim 2\%$  in the Rainbow Basin stratigraphic section.

Second, the observed rates of change in calcite  $\delta^{18}\text{O}$  values for the Soledad Basin (Fig. 2A), Rainbow Basin (Fig. 2B), Death Valley area (Fig. 2C), and western Arizona (Fig. 2E) isotope records are significantly different than the rates of change for both calcite and smectite  $\delta^{18}\text{O}$  values in the El Paso Basin isotopic record (Poage and Chamberlain, 2002; Fig. 2F). The rates at which authigenic mineral  $\delta^{18}\text{O}$  values increase in the El Paso Basin (Fig. 2F) are  $\sim 2$ – $3$  times faster ( $1.2\%$  smectite  $\delta^{18}\text{O}$  per million years;  $0.74\%$  calcite  $\delta^{18}\text{O}$  per million years) than the rates observed elsewhere in the central Basin and Range Province ( $0.09\%$  to  $0.39\%$  calcite  $\delta^{18}\text{O}$  per million years; Fig. 2A–E) and the western and northern Great Basin ( $0.19\%$  and  $0.36\%$  calcite  $\delta^{18}\text{O}$  per million years; Fig. 2F).

Third, in the Lake Mead Basin, an  $\sim 5\%$  decrease in calcite  $\delta^{18}\text{O}$  values is recognized within the Horse Spring Formation between ca. 25 and ca. 13 Ma (Fig. 2D). This is the only Great Basin isotopic record that exhibits a

decrease in calcite  $\delta^{18}\text{O}$  values during the Oligocene to Miocene, suggesting a local mechanism is responsible for this isotopic shift.

Fourth, smectite  $\delta^{18}\text{O}$  values in the Rainbow Basin are generally  $\sim 5\%$  lower than the adjacent calcites during the middle Miocene (Fig. 2B). Based on temperature-dependent mineral-water fractionation equations (calcite—Kim and O'Neil, 1997; smectite—Sheppard and Gilg, 1996), authigenic smectite and calcite  $\delta^{18}\text{O}$  values should be offset by  $\sim 3\%$ , with smectite having the lower  $\delta$  values, assuming both minerals formed in isotopic equilibrium with the same water at the same temperature (Poage and Chamberlain, 2002). Thus, the  $\sim 5\%$  offset between smectite and calcite  $\delta^{18}\text{O}$  values is most likely due to differences in the isotopic composition of surface waters present during the time of mineral formation, and/or differences in the temperatures at which calcite and smectite formed.

Fifth, smectite  $\delta^{18}\text{O}$  and  $\delta\text{D}$  values from the Rainbow Basin and El Paso Basin stratigraphic sections plot in a distribution subparallel to the stable isotopic global meteoric water line (Fig. 3). This distribution is significantly different from the distribution of smectite  $\delta^{18}\text{O}$  and  $\delta\text{D}$  values defined by samples from the western and northern Great Basin, which plot roughly parallel to the global meteoric water line (Fig. 3). This difference is most likely the result of evaporative modification of the surface waters present during the time of smectite formation in the El Paso and Rainbow Basin stratigraphic sections.

Sixth, with the exception of the El Paso Basin record of Poage and Chamberlain (2002), authigenic mineral  $\delta^{18}\text{O}$  values in the central Basin and Range Province area are  $\sim 6\%$  higher than similar-age authigenic mineral  $\delta^{18}\text{O}$  values from the northern and western Great Basin sections of Poage and Chamberlain (2002) and Horton et al. (2004) (Fig. 4). This offset is roughly the same magnitude as the difference in modern precipitation  $\delta^{18}\text{O}$  values between southern California and northern Nevada (Fig. 1) (Friedman et al., 2002b). El Paso Basin smectite and calcite  $\delta^{18}\text{O}$  values plot in between the northern Great Basin and central Basin and Range Province end members (Fig. 4), despite geographic proximity to the central Basin and Range Province basins investigated here (Fig. 1). The anomalous nature of the El Paso isotopic record suggests a local mechanism is responsible for the relatively rapid  $\sim 5\%$  shift in smectite and calcite  $\delta^{18}\text{O}$  values observed in this basin.

Seventh, there is a general lack of covariance between calcite  $\delta^{13}\text{C}$  and  $\delta^{18}\text{O}$  values in the lacustrine carbonates investigated (Fig. 5), with the notable exception of strong isotopic covariance within the limestone Ubehebe Formation (Fig. 5C) and the Thumb Member of the Horse

## NEOGENE PALEOTOPOGRAPHY OF THE CENTRAL BASIN AND RANGE PROVINCE

TABLE 1. AUTHIGENIC CALCITE GEOCHEMICAL DATA

Basin/sample	Geologic formation	Latitude (°N)	Longitude (°W)	$\delta^{18}\text{O}$ (‰, PDB)	$\delta^{13}\text{C}$ (‰, PDB)	Mg/Ca	Mn/Ca ( $\times 10^4$ )	Sr/Ca ( $\times 10^3$ )
<u>Soledad Basin</u>								
SR/CA-08-03	Saugus (Sunshine Ranch Mbr)	34.3990	118.4776	-6.3	-11.2			
SR/CA-09-03	Saugus (Sunshine Ranch Mbr)	34.3990	118.4776	-8.2	-11.8			
SR/CA-11-03	Saugus (Sunshine Ranch Mbr)	34.3990	118.4776	-6.8	-10.5			
SR/CA-12-03	Saugus (Sunshine Ranch Mbr)	34.3990	118.4776	-5.5	-9.9			
SR/CA-13-03	Saugus (Sunshine Ranch Mbr)	34.3990	118.4776	-6.8	-13.5			
MC/CA-03-11	Mint Canyon	34.4895	118.5163	-10.2	-5.3			
MC/CA-03-12	Mint Canyon	34.4895	118.5163	-8.8	-5.6			
MC/CA-03-13	Mint Canyon	34.4895	118.5163	-10.5	-6.0			
VQ/CA-03-06	Vasquez	34.4775	118.3566	-10.7	-9.9			
VQ/CA-03-08	Vasquez	34.4775	118.3566	-12.9	-6.6			
VQ/CA-03-14	Vasquez	34.4775	118.3566	-14.2	-13.4			
VQ/CA-03-16	Vasquez	34.4775	118.3566	-9.6	-13.8			
VQ/CA-03-18	Vasquez	34.4775	118.3566	-11.9	-8.0			
<u>Rainbow Basin</u>								
BF-18	Middle Barstow	35.0223	117.0346	-6.2	-2.2	0.002	1.7	1.2
BF-20	Middle Barstow	35.0223	117.0346	-8.7	-3.5	0.0004	14.6	4.9
BF-27	Middle Barstow	35.0223	117.0346	-7.6	-3.7	0.023	4.8	6.4
BF-31	Middle Barstow	35.0223	117.0346	-6.7	-2.5			
BF-36	Middle Barstow	35.0223	117.0346	-6.0	1.1	0.062	4.7	6.4
BF-38	Middle Barstow	35.0223	117.0346	-6.9	-4.3	0.019	8.8	6.3
BF-39	Middle Barstow	35.0223	117.0346	-7.2	-1.5	0.003	0.5	7.1
BF-40	Middle Barstow	35.0223	117.0346	-6.6	-1.5			
BF-01	Lower Barstow	35.0223	117.0346	-8.4	-1.5	0.002	1.3	2.7
BF-02	Lower Barstow	35.0223	117.0346	-8.7	-3.5	0.001	0.7	0.4
BF-09	Lower Barstow	35.0223	117.0346	-8.0	-0.1	0.001	9.2	1.3
BF-10	Lower Barstow	35.0223	117.0346	-7.1	-1.4	0.003	14.6	2.2
BF-14	Lower Barstow	35.0223	117.0346	-8.8	-5.7	0.001	3.8	1.7
BF-15	Lower Barstow	35.0223	117.0346	-9.1	-2.0	0.001	9.6	0.8
<u>Death Valley</u>								
ZP-3	Furnace Creek	36.4231	116.8279	-6.9	0.1			
ZP-4	Furnace Creek	36.4231	116.8279	-5.8	0.6			
ZP-5	Furnace Creek	36.4231	116.8279	-7.7	0.7			
ZP-6	Furnace Creek	36.4231	116.8279	-7.1	-0.5			
ZP-7	Furnace Creek	36.4231	116.8279	-5.4	0.0			
ZP-10	Furnace Creek	36.4231	116.8279	-8.9	0.0	0.032	1.1	1.7
ZP-12	Furnace Creek	36.4231	116.8279	-9.5	3.2			
ZP-13	Furnace Creek	36.4231	116.8279	-6.1	0.1			
ZP-14	Furnace Creek	36.4231	116.8279	-5.3	-0.6			
ZP-15	Furnace Creek	36.4231	116.8279	-6.4	-0.6			
ZP-18	Furnace Creek	36.4231	116.8279	-7.4	4.0			
ZP-19	Furnace Creek	36.4231	116.8279	-8.8	2.9			
ZP-21	Furnace Creek	36.4231	116.8279	-7.7	4.6			
ZP-22	Furnace Creek	36.4231	116.8279	-9.4	4.7			
ZP-24	Furnace Creek	36.4231	116.8279	-9.6	3.5			
ZP-26	Furnace Creek	36.4231	116.8279	-6.9	2.2			
ZP-28	Furnace Creek	36.4231	116.8279	-6.9	1.9			
ZP-30	Furnace Creek	36.4231	116.8279	-5.0	1.0	0.045	7.1	1.7
ZP-32	Furnace Creek	36.4231	116.8279	-10.0	0.3			
CW/CA-01	Panuga	36.5633	117.3324	-10.6	-2.4			
CW/CA-03	Panuga	36.5633	117.3324	-9.2	-0.5			
CW/CA-05	Panuga	36.5633	117.3324	-9.8	-0.8			
CW/CA-08	Panuga	36.5633	117.3324	-9.3	-2.5	0.004	3.6	0.9
CW/CA-10	Panuga	36.5633	117.3324	-10.5	-1.9	0.002	0.0	0.3
CW/CA-11	Panuga	36.5633	117.3324	-10.3	-1.9	0.018	0.7	0.2
BM-25	Bat Mountain (Kelley's Well Limestone Mbr)	36.3882	116.5174	-15.2	0.5	0.002	0.1	0.1
BM-26	Bat Mountain (Kelley's Well Limestone Mbr)	36.3882	116.5174	-16.3	0.4	0.06	12.3	0.5
BM-27	Bat Mountain (Kelley's Well Limestone Mbr)	36.3882	116.5174	-16.5	1.0	0.002	0.0	0.4
BM-28	Bat Mountain (Kelley's Well Limestone Mbr)	36.3882	116.5174	-12.8	-1.4			
BM-29	Bat Mountain (Kelley's Well Limestone Mbr)	36.3882	116.5174	-16.0	2.6			
BM-30	Bat Mountain (Kelley's Well Limestone Mbr)	36.3882	116.5174	-15.7	1.0			
BM-31	Bat Mountain (Kelley's Well Limestone Mbr)	36.3882	116.5174	-15.4	1.2			
BM-32	Bat Mountain (Kelley's Well Limestone Mbr)	36.3882	116.5174	-15.7	1.4			
BM-33	Bat Mountain (Kelley's Well Limestone Mbr)	36.3882	116.5174	-14.8	1.4			

(continued)

TABLE 1. AUTHIGENIC CALCITE GEOCHEMICAL DATA (continued)

Basin/sample	Geologic formation	Latitude (°N)	Longitude (°W)	$\delta^{18}\text{O}$ (‰, PDB)	$\delta^{13}\text{C}$ (‰, PDB)	Mg/Ca	Mn/Ca ( $\times 10^4$ )	Sr/Ca ( $\times 10^3$ )
BM-1	Ubehebe (limestone)	36.3882	116.5174	-13.8	-4.5			
BM-2	Ubehebe (limestone)	36.3882	116.5174	-13.3	-4.5			
BM-3	Ubehebe (limestone)	36.3882	116.5174	-14.4	-5.2	0.011	0.5	0.5
BM-4	Ubehebe (limestone)	36.3882	116.5174	-12.2	-4.0			
BM-5	Ubehebe (limestone)	36.3882	116.5174	-16.5	-5.7			
BM-6	Ubehebe (limestone)	36.3882	116.5174	-14.3	-5.4	0.003	0.5	0.3
BM-8	Ubehebe (limestone)	36.3882	116.5174	-12.8	-4.9			
BM-9	Ubehebe (limestone)	36.3882	116.5174	-14.7	-5.6			
BM-10	Ubehebe (limestone)	36.3882	116.5174	-15.9	-5.4	0.004	0.4	0.1
BM-12	Ubehebe (limestone)	36.3882	116.5174	-12.0	-3.8			
BM-13	Ubehebe (limestone)	36.3882	116.5174	-15.2	-5.6	0.001	2.5	0.1
BM-14	Ubehebe (limestone)	36.3882	116.5174	-15.6	-5.3			
BM-20	Ubehebe (limestone)	36.3882	116.5174	-15.1	-5.2			
Lake Mead Area								
MC-2	Muddy Creek	35.9646	114.3468	-12.0	0.9			
MC-3	Muddy Creek	35.9646	114.3468	-11.8	-0.1			
MC-6	Muddy Creek	35.9646	114.3468	-12.5	1.5			
MC-7	Muddy Creek	35.9646	114.3468	-12.9	2.0			
MC-9	Muddy Creek	35.9646	114.3468	-12.6	1.7			
MC-10	Muddy Creek	35.9646	114.3468	-12.6	1.7			
MC-11	Muddy Creek	35.9646	114.3468	-12.3	1.3			
MC-12	Muddy Creek	35.9646	114.3468	-12.3	0.8			
MC-13	Muddy Creek	35.9646	114.3468	-11.2	1.2			
MC-14	Muddy Creek	35.9646	114.3468	-12.3	0.5			
LW-29	Horse Spring—Lovell Wash Mbr	36.1583	114.9086	-12.5	7.9			
LW-30	Horse Spring—Lovell Wash Mbr	36.1583	114.9086	-12.2	5.7			
LW-34	Horse Spring—Lovell Wash Mbr	36.1583	114.9086	-11.2	3.6			
LW-38	Horse Spring—Lovell Wash Mbr	36.1583	114.9086	-11.6	10.8			
LW-40	Horse Spring—Lovell Wash Mbr	36.1583	114.9086	-13.1	0.4			
BR-01	Horse Spring—Bitter Ridge Mbr	36.1405	114.9500	-11	0.6			
BR-02	Horse Spring—Bitter Ridge Mbr	36.1405	114.9500	-11.5	0.3			
BR-03	Horse Spring—Bitter Ridge Mbr	36.1405	114.9500	-11.2	0.8			
BR-04A	Horse Spring—Bitter Ridge Mbr	36.1405	114.9500	-12.4	0.6			
BR-05	Horse Spring—Bitter Ridge Mbr	36.1405	114.9500	-11.4	0.4			
BR-06	Horse Spring—Bitter Ridge Mbr	36.1405	114.9500	-11.6	0.4			
BR-07	Horse Spring—Bitter Ridge Mbr	36.1405	114.9500	-13.6	0.7			
BR-08	Horse Spring—Bitter Ridge Mbr	36.1405	114.9500	-12.1	1.4			
BR-09	Horse Spring—Bitter Ridge Mbr	36.1405	114.9500	-7.7	0.1			
BR-10	Horse Spring—Bitter Ridge Mbr	36.1405	114.9500	-10.7	0			
BR-11	Horse Spring—Bitter Ridge Mbr	36.1405	114.9500	-12.4	0.8			
BR-12	Horse Spring—Bitter Ridge Mbr	36.1405	114.9500	-12	0.9			
BR-13	Horse Spring—Bitter Ridge Mbr	36.1405	114.9500	-13	0.7			
BR-15	Horse Spring—Bitter Ridge Mbr	36.1405	114.9500	-7	0.1			
BR-21	Horse Spring—Bitter Ridge Mbr	36.1405	114.9500	-14.1	0.6			
BR-22	Horse Spring—Bitter Ridge Mbr	36.1405	114.9500	-12.7	0.4			
BR-23	Horse Spring—Bitter Ridge Mbr	36.1405	114.9500	-12.2	0.2			
BR-24	Horse Spring—Bitter Ridge Mbr	36.1405	114.9500	-11.8	0.2			
BR-25	Horse Spring—Bitter Ridge Mbr	36.1405	114.9500	-11.5	0.7			
BR-26	Horse Spring—Bitter Ridge Mbr	36.1405	114.9500	-12.4	0.8			
BR-27	Horse Spring—Bitter Ridge Mbr	36.1405	114.9500	-11.9	0.7			
BR-28	Horse Spring—Bitter Ridge Mbr	36.1405	114.9500	-10.4	0.8			
TH-16	Horse Spring—Thumb Mbr	36.1432	114.9524	-9.1	-1.7			
TH-17	Horse Spring—Thumb Mbr	36.1432	114.9524	-10.2	-1.4			
TH-18	Horse Spring—Thumb Mbr	36.1432	114.9524	-10.1	-2.7			
TH-19A	Horse Spring—Thumb Mbr	36.1432	114.9524	-11.2	-4.1			
TH-19B	Horse Spring—Thumb Mbr	36.1432	114.9524	-10.7	-3.8			
TH-21	Horse Spring—Thumb Mbr	36.1432	114.9524	-9.9	-3.6			
TH-22	Horse Spring—Thumb Mbr	36.1432	114.9524	-10.6	-3.6			
TH-23	Horse Spring—Thumb Mbr	36.1432	114.9524	-9.2	-3.2			
TH-24	Horse Spring—Thumb Mbr	36.1432	114.9524	-7.7	-1.9			
TH-25	Horse Spring—Thumb Mbr	36.1432	114.9524	-9.8	-2.8			
TH-28	Horse Spring—Thumb Mbr	36.1432	114.9524	-9.8	-2.9			
TH-29	Horse Spring—Thumb Mbr	36.1432	114.9524	-8.7	-0.4			
TH-30	Horse Spring—Thumb Mbr	36.1432	114.9524	-8.8	0.1			

(continued)

## NEOGENE PALEOTOPOGRAPHY OF THE CENTRAL BASIN AND RANGE PROVINCE

TABLE 1. AUTHIGENIC CALCITE GEOCHEMICAL DATA (continued)

Basin/sample	Geologic formation	Latitude (°N)	Longitude (°W)	$\delta^{18}\text{O}$ (‰, PDB)	$\delta^{13}\text{C}$ (‰, PDB)	Mg/Ca	Mn/Ca ( $\times 10^4$ )	Sr/Ca ( $\times 10^3$ )
TH-31	Horse Spring—Thumb Mbr	36.1432	114.9524	-8.7	-0.1			
TH-32	Horse Spring—Thumb Mbr	36.1432	114.9524	-7.8	0.7			
TH-33	Horse Spring—Thumb Mbr	36.1432	114.9524	-9.3	-0.9			
TH-34	Horse Spring—Thumb Mbr	36.1432	114.9524	-8.5	-0.1			
TH-35	Horse Spring—Thumb Mbr	36.1432	114.9524	-6.1	1.8			
TH-36A	Horse Spring—Thumb Mbr	36.1432	114.9524	-6.3	1.5			
TH-37	Horse Spring—Thumb Mbr	36.1432	114.9524	-12.3	-3.8			
TH-38	Horse Spring—Thumb Mbr	36.1432	114.9524	-11.6	-4.1			
TH-39	Horse Spring—Thumb Mbr	36.1432	114.9524	-11.8	-2.4			
TH-40	Horse Spring—Thumb Mbr	36.1432	114.9524	-10.8	-3.3			
RG-17	Horse Spring—Upper Rainbow Gardens Mbr	36.3511	114.1341	-10.8	5			
RG-18	Horse Spring—Upper Rainbow Gardens Mbr	36.3511	114.1341	-10.1	3.6			
RG-19	Horse Spring—Upper Rainbow Gardens Mbr	36.3511	114.1341	-10	1.5			
RG-20	Horse Spring—Upper Rainbow Gardens Mbr	36.3511	114.1341	-10.2	2.6			
RG-21	Horse Spring—Upper Rainbow Gardens Mbr	36.3511	114.1341	-10	3.6			
RG-22	Horse Spring—Upper Rainbow Gardens Mbr	36.3511	114.1341	-9.8	4.1			
RG-23	Horse Spring—Upper Rainbow Gardens Mbr	36.3511	114.1341	-10.5	3.5			
RG-24	Horse Spring—Upper Rainbow Gardens Mbr	36.3511	114.1341	-9	2.1			
RG-25	Horse Spring—Upper Rainbow Gardens Mbr	36.3511	114.1341	-10.7	2			
RG-26	Horse Spring—Upper Rainbow Gardens Mbr	36.3511	114.1341	-10.6	3			
RG-27	Horse Spring—Upper Rainbow Gardens Mbr	36.3511	114.1341	-9.7	2.9			
RG-28	Horse Spring—Upper Rainbow Gardens Mbr	36.3511	114.1341	-9.5	2.4			
RG-29	Horse Spring—Upper Rainbow Gardens Mbr	36.3511	114.1341	-9.7	3.3			
RG-30	Horse Spring—Upper Rainbow Gardens Mbr	36.3511	114.1341	-10.1	3.3			
RG-31	Horse Spring—Upper Rainbow Gardens Mbr	36.3511	114.1341	-9.7	1.9			
RG-32	Horse Spring—Upper Rainbow Gardens Mbr	36.3511	114.1341	-10.2	0.9			
RG-33	Horse Spring—Upper Rainbow Gardens Mbr	36.3511	114.1341	-8.8	3.6			
RG-34	Horse Spring—Upper Rainbow Gardens Mbr	36.3511	114.1341	-9.3	2.3			
RG-35	Horse Spring—Upper Rainbow Gardens Mbr	36.3511	114.1341	-9.7	3.3			
RG-36	Horse Spring—Upper Rainbow Gardens Mbr	36.3511	114.1341	-9.1	2.7			
RG-37	Horse Spring—Upper Rainbow Gardens Mbr	36.3511	114.1341	-9.2	2.7			
RG-38	Horse Spring—Upper Rainbow Gardens Mbr	36.3511	114.1341	-9.4	3.9			
RG-39	Horse Spring—Upper Rainbow Gardens Mbr	36.3511	114.1341	-9.4	3			
RG-40	Horse Spring—Upper Rainbow Gardens Mbr	36.3511	114.1341	-10.5	3.2			
RG-42	Horse Spring—Upper Rainbow Gardens Mbr	36.3511	114.1341	-9.7	1.9			
RG-43	Horse Spring—Upper Rainbow Gardens Mbr	36.3511	114.1341	-9.2	1.5			
RG-37.1	Horse Spring—Upper Rainbow Gardens Mbr	36.3511	114.1341	-4.5	2.7			
RG-38.1	Horse Spring—Upper Rainbow Gardens Mbr	36.3511	114.1341	-4.2	1.6			
RG-39.1	Horse Spring—Upper Rainbow Gardens Mbr	36.3511	114.1341	-3.9	0.5			
RG-40.1	Horse Spring—Upper Rainbow Gardens Mbr	36.3511	114.1341	-9.1	-0.2			
RG-40B.1	Horse Spring—Upper Rainbow Gardens Mbr	36.3511	114.1341	-3.8	0.5			
RG-42.1	Horse Spring—Upper Rainbow Gardens Mbr	36.3511	114.1341	-3.9	0.2			
HS-03	Horse Spring—Lower Rainbow Gardens Mbr	36.1438	114.9572	-9.6	1.5			
HS-05	Horse Spring—Lower Rainbow Gardens Mbr	36.1438	114.9572	-9.9	1.7			
HS-07	Horse Spring—Lower Rainbow Gardens Mbr	36.1438	114.9572	-8.0	0.2			
HS-08	Horse Spring—Lower Rainbow Gardens Mbr	36.1438	114.9572	-8.9	-0.7			
HS-10	Horse Spring—Lower Rainbow Gardens Mbr	36.1438	114.9572	-7.5	0.3			
HS-11	Horse Spring—Lower Rainbow Gardens Mbr	36.1438	114.9572	-8.8	-1.0			
HS-13	Horse Spring—Lower Rainbow Gardens Mbr	36.1438	114.9572	-8.3	-1.5			
HS-15	Horse Spring—Lower Rainbow Gardens Mbr	36.1438	114.9572	-6.8	-4.3			
HS-16	Horse Spring—Lower Rainbow Gardens Mbr	36.1438	114.9572	-5.4	-0.3			
RG-01	Horse Spring—Lower Rainbow Gardens Mbr	36.1438	114.9572	-1.1	1			
RG-03	Horse Spring—Lower Rainbow Gardens Mbr	36.1438	114.9572	-1.9	1.5			
RG-04	Horse Spring—Lower Rainbow Gardens Mbr	36.1438	114.9572	-2.9	2.2			
RG-05	Horse Spring—Lower Rainbow Gardens Mbr	36.1438	114.9572	-4.9	1.8			
RG-09	Horse Spring—Lower Rainbow Gardens Mbr	36.1438	114.9572	-1.8	5			
RG-11	Horse Spring—Lower Rainbow Gardens Mbr	36.1438	114.9572	-10.4	2.6			
RG-12	Horse Spring—Lower Rainbow Gardens Mbr	36.1438	114.9572	-10.4	2.8			
RG-13	Horse Spring—Lower Rainbow Gardens Mbr	36.1438	114.9572	-9.9	1.7			
RG-14	Horse Spring—Lower Rainbow Gardens Mbr	36.1438	114.9572	-4.3	4.8			
RG-15	Horse Spring—Lower Rainbow Gardens Mbr	36.1438	114.9572	-10.4	7			
RG-16	Horse Spring—Lower Rainbow Gardens Mbr	36.1438	114.9572	-10.2	-0.7			

(continued)

TABLE 1. AUTHIGENIC CALCITE GEOCHEMICAL DATA (continued)

Basin/sample	Geologic formation	Latitude (°N)	Longitude (°W)	δ <sup>18</sup> O (‰, PDB)	δ <sup>13</sup> C (‰, PDB)	Mg/Ca	Mn/Ca (×10 <sup>4</sup> )	Sr/Ca (×10 <sup>3</sup> )
<b>Western Arizona</b>								
BC-1	Artillery	34.5467	113.5847	-8.8	-5.0			
BC-2	Artillery	34.5467	113.5847	-7.9	-4.9			
BC-5	Artillery	34.5467	113.5847	-10.3	-4.0			
BC-6	Artillery	34.5467	113.5847	-10.7	-2.7			
BC-16	Artillery	34.5467	113.5847	-8.2	-3.2			
BS-2	Big Sandy	34.6374	113.5547	-5.0	2.5			
BS-5	Big Sandy	34.6374	113.5547	-6.5	0.6			
BS-7	Big Sandy	34.6374	113.5547	-8.5	0.9			
BS-9g	Big Sandy	34.6374	113.5547	-6.6	0.8			
BS-10	Big Sandy	34.6374	113.5547	-7.5	-3.5			
BS-11	Big Sandy	34.6374	113.5547	-6.6	-1.0			
BS-12	Big Sandy	34.6374	113.5547	-6.4	-5.0			
BS-13	Big Sandy	34.6374	113.5547	-8.4	-3.6			

Note: PDB—Peedee belemnite.

Spring Formation (Fig. 5D). Strong covariance ( $R^2 > 0.7$ ) between lacustrine carbonate δ<sup>13</sup>C and δ<sup>18</sup>O values is indicative of hydrologically closed basins and has been recognized in both modern and ancient settings (Talbot, 1990).

**DISCUSSION**

Stable isotope-based paleotopographic investigations are based upon the observation that the isotopic composition of precipitation on the leeward side of mountain ranges is strongly correlated with relief (Dansgaard, 1964; Chamberlain and Poage, 2000; Rowley et al., 2001). This altitude effect was quantified by a compilation of precipitation and surface-water stable isotopic data sets which show an ~-2.8‰ δ<sup>18</sup>O water/km of elevation increase globally (Poage

and Chamberlain, 2001). This finding suggests that the paleotopographic history of mountain belts can be evaluated using the oxygen isotope composition of authigenic minerals forming in isotopic equilibrium with unmodified surface waters (Chamberlain and Poage, 2000; Rowley et al., 2001). Several recent investigations have applied this paleotopographic proxy method to world mountain belts, including the Southern Alps of New Zealand (Chamberlain et al., 1999), the Himalaya and Tibetan Plateau (e.g., Garzzone et al., 2000; Rowley et al., 2001; Dettman et al., 2003), and the Sierra Nevada (Poage and Chamberlain, 2002).

In order to isolate the effects of topography on the authigenic mineral stable isotopic records presented here, several factors that influence the isotopic composition of authi-

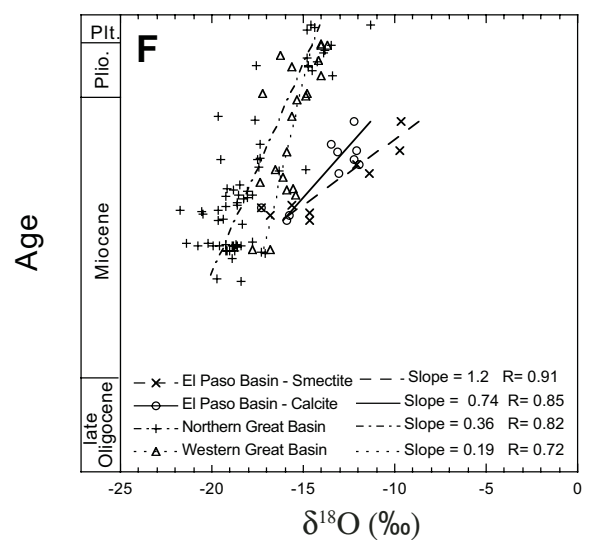
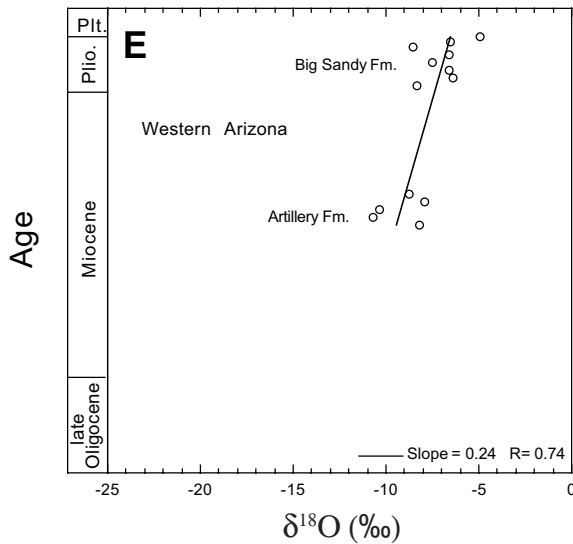
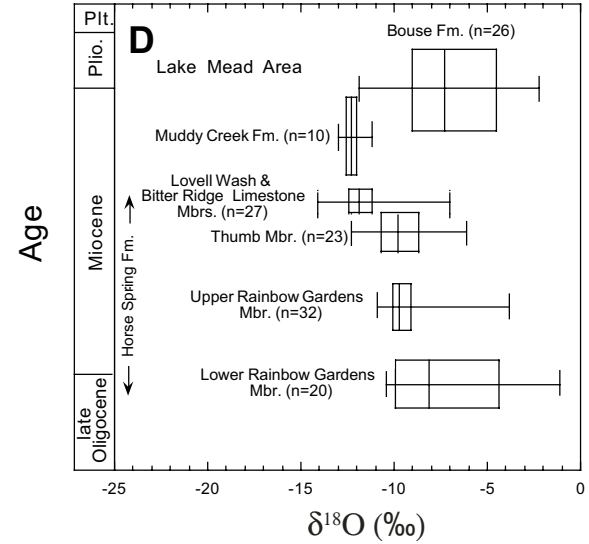
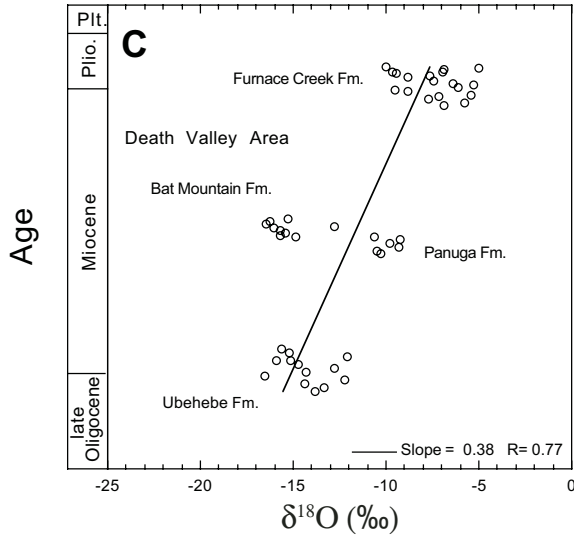
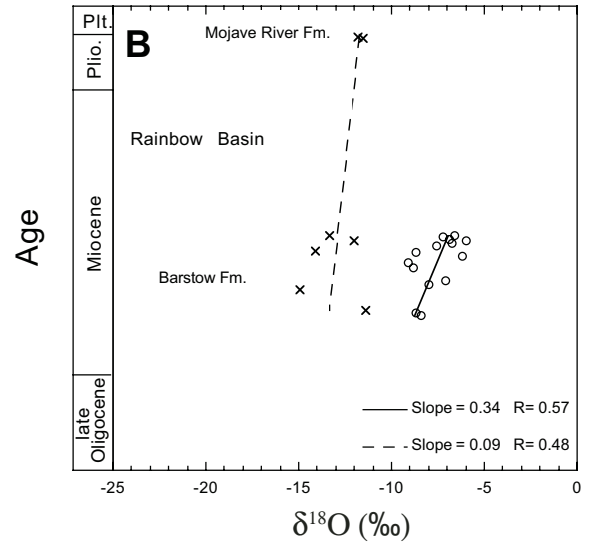
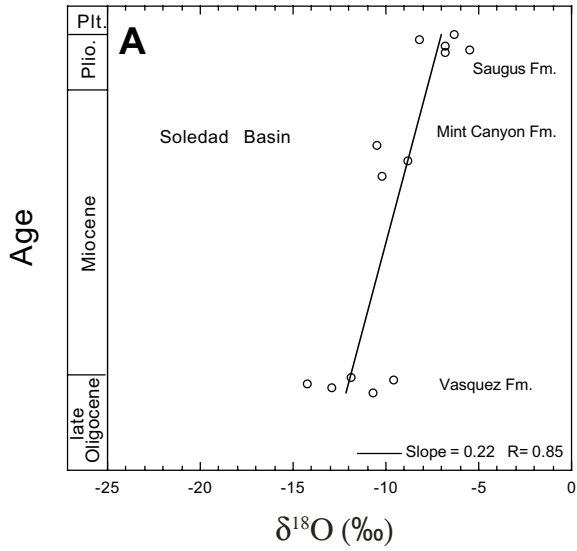
genic minerals must also be considered. These factors include: changes in latitude, longitude, temperature, evaporation, diagenesis, and surface-water source region. Following a detailed consideration of these factors, we suggest that the general pattern of increasing authigenic mineral δ<sup>18</sup>O values with decreasing age since the middle Miocene recognized throughout the central Basin and Range Province results from one or both of the following mechanisms: (1) regional topographic lowering of ~1–3 km associated with widespread crustal extension since 20 Ma; and (2) prolonged regional cooling and aridification since the middle Miocene. We further suggest that the observed decrease in calcite δ<sup>18</sup>O values in the Lake Mead Basin between ca. 25 Ma and ca. 13 Ma results from an ~1.5 km surface uplift event associated with

TABLE 2. SMECTITE STABLE ISOTOPE DATA

Basin/sample	Geologic formation	Age (Ma)	δ <sup>18</sup> O (‰, SMOW)	δ <sup>18</sup> O (‰, PDB)	δD (‰, SMOW)
<b>Rainbow Basin</b>					
MD/CA-12	Mojave River	2.0	18.8	-11.8	—
MD/CA-11	Mojave River	2.1	19.1	-11.5	-102
MD/CA-07	Middle Barstow	14.8	17.2	-13.3	-103
BF-36	Middle Barstow	15.2	18.6	-12.0	-104
BF-24	Middle Barstow	15.8	16.4	-14.1	-110
BF-05	Lower Barstow	19.3	15.6	-14.9	-99
MD/CA-20	Lower Barstow	19.7	19.2	-11.4	-96
<b>El Paso Basin</b>					
EPB-7	Dove Spring	7.0	21	-10.5	-102
EPB-6	Dove Spring	8.9	20.9	-10.6	-105
EPB-3	Dove Spring	9.8	18.5	-13.0	-102
EPB-13	Dove Spring	12.5	14.8	-16.6	-110
EPB-11	Dove Spring	13.0	15.8	-15.6	-106
EPB-10	Dove Spring	13.2	13.6	-17.7	-111
EPB-9	Dove Spring	13.5	15.9	-15.5	-111

Note: PDB—Peedee belemnite; SMOW—standard mean ocean water.

Figure 2. Authigenic mineral δ<sup>18</sup>O records. Calcites are shown as open circles and smectites as multiplication signs in A, B, C, and E. (A) Authigenic calcite δ<sup>18</sup>O record for the Soledad Basin. (B) Authigenic calcite and smectite δ<sup>18</sup>O records for the Rainbow Basin. (C) Authigenic calcite δ<sup>18</sup>O record for the Death Valley area. (D) Authigenic calcite whiskered quartile boxes for lithostratigraphic units sampled from the Lake Mead area (Bouse Formation data from Poulson and John, 2003). (E) Authigenic calcite δ<sup>18</sup>O record for the western Arizona area. (F) Authigenic calcite and smectite δ<sup>18</sup>O records for the El Paso Basin (calcite—open circles; smectite—multiplication signs), western Great Basin (calcite and smectite—open triangles), and northern Great Basin (calcite and smectite—addition signs). Plio.—Pliocene; Pli.—Pleistocene.



magmatic activity in the eastern central Basin and Range Province during this time.

**Latitude and Longitude Effects**

Craig (1961) presented a detailed description of the correlation between the isotopic

composition of precipitation and latitude. This paper was the first investigation to document the correlation between the hydrogen and oxygen isotopic composition of precipitation (i.e., the global meteoric water line) at different latitudes, with high-latitude regions characterized by precipitation with lower  $\delta D$  and  $\delta^{18}O$  values than

lower-latitude regions. However, changes in latitude did not significantly affect the isotopic values presented here, as the western United States has remained at approximately the same latitude throughout the Cenozoic era (Smith et al., 1981). Similarly, the in-land distance an air mass travels, or longitude effect, also causes a relative depletion of D and  $^{18}O$  in precipitation. Longitudinal isotopic effects are also minor in the current investigation, as even a 200 km increase in the distance to shore, roughly the distance from Death Valley to the California coast, since the middle Miocene would only result in a 0.4‰ increase in  $\delta^{18}O$  precipitation values relative to modern, assuming a longitude isotopic lapse rate of 0.002‰  $\delta^{18}O$  precipitation/km (Criss, 1999).

**Temperature Effects**

To quantify the effect of temperature on the produced authigenic mineral isotopic records, calcite  $\delta^{18}O$  values were calculated by applying the effect of a 5 °C temperature increase relative to modern to both the calcite-water fractionation factor and the isotopic composition of precipitation in the central Basin and Range (Friedman et al., 1992). A 5 °C increase was chosen because this is the approximate amount of global cooling that has occurred since the middle Miocene climatic optimum, based on marine climate records (Zachos et al., 2001). Modern precipitation in the central Basin and Range has a representative  $\delta^{18}O$  value of  $\sim -7\text{‰}$  (Friedman et al., 1992), and mean annual temperature in the region is  $\sim 18\text{ °C}$ . Applying these values to the calcite-water fractionation equation of Kim and O’Neil (1997) yields a calculated modern calcite  $\delta^{18}O$  value of  $-8.2\text{‰}$  for the central Basin and Range. Seasonal variations in modern air temperatures are extreme in the central Basin and Range, with summer average highs of  $\sim 35\text{ °C}$  and winter average lows of  $\sim 7\text{ °C}$ . Applying this seasonal range in temperature to the calcite-water fractionation equation results in an  $\sim \pm 2.5\text{‰}$  range in calculated calcite  $\delta^{18}O$  values. This range in calculated values,  $-8.2 \pm 2.5\text{‰}$ , agrees well with the youngest authigenic calcite  $\delta^{18}O$  values recognized in the stable isotopic records presented here (Fig. 4). Doing a similar calculation at 23 °C, after correcting the isotopic composition of precipitation for both the change in temperature (using the  $0.58\text{‰/°C}$  lapse rate of Rozanski et al., 1993) and the effects of changes in ice-sheet volume since the middle Miocene (from Zachos et al., 2001), yields a calculated middle Miocene authigenic calcite  $\delta^{18}O$  value of  $-8.0\text{‰}$ . Based on this calculation set, a 5 °C decrease in regional temperature since the middle Miocene would result in an  $\sim 0.2\text{‰}$  increase

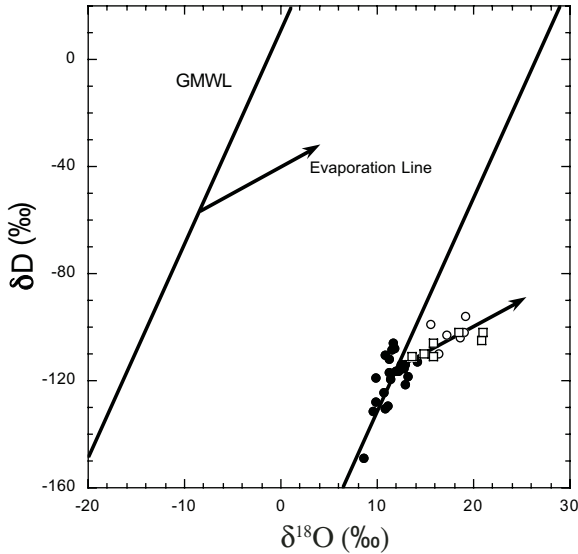


**Figure 3.** Smectite  $\delta D$  versus  $\delta^{18}O$  values for the northern Great Basin (filled circles) and the central Basin and Range Province (El Paso Basin section—squares; Rainbow Basin section—open circles). GMWL—global meteoric water line.

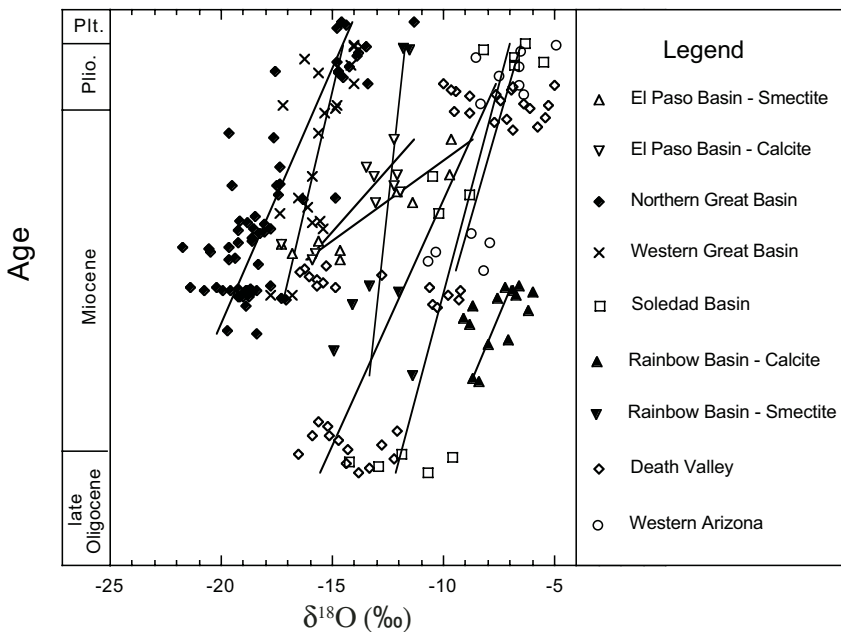


**Figure 4.** Authigenic mineral  $\delta^{18}O$  records for all sections investigated except the Lake Mead Basin. Plio.—Pliocene; Plt.—Pleistocene.

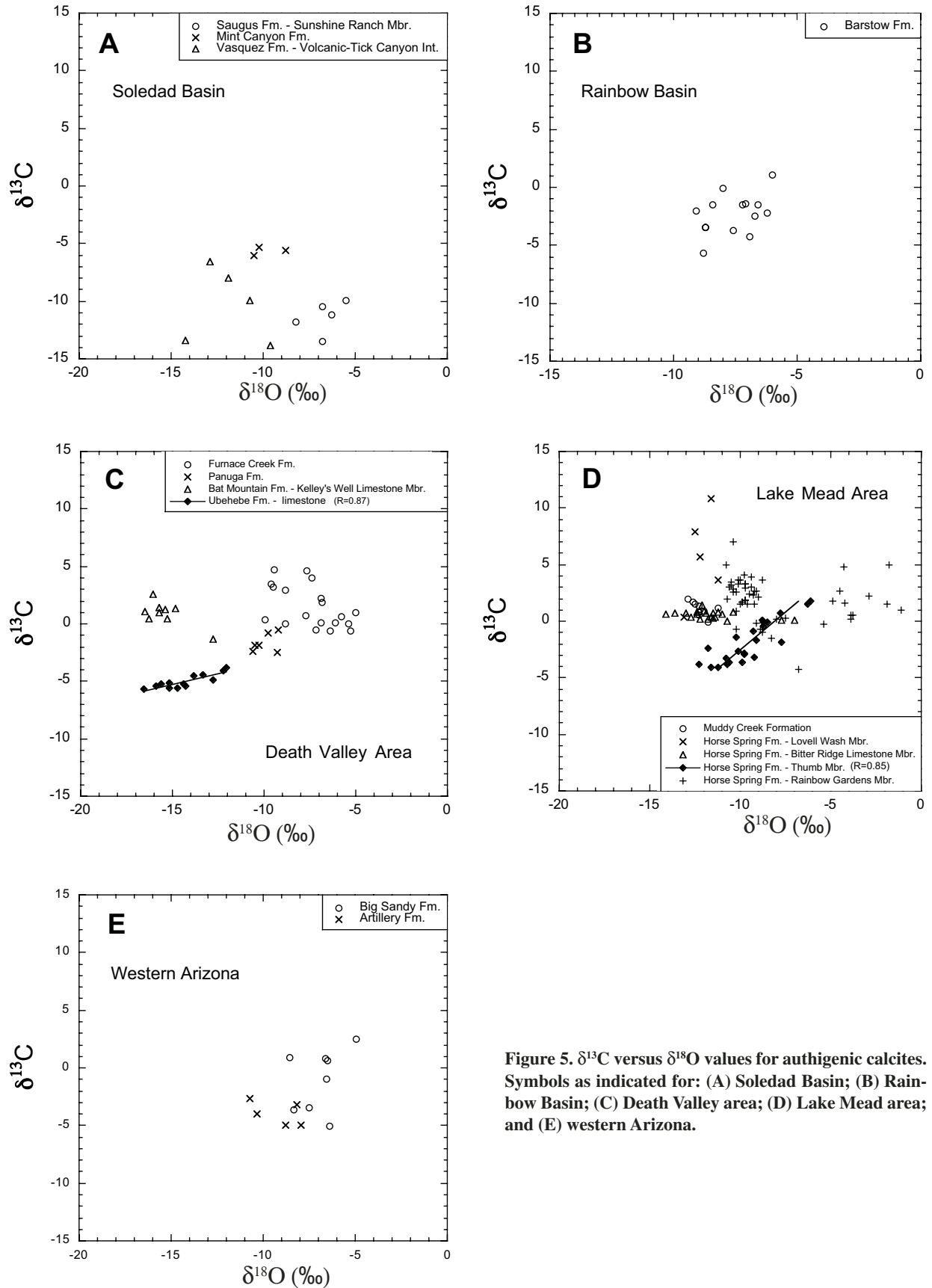


Figure 5.  $\delta^{13}\text{C}$  versus  $\delta^{18}\text{O}$  values for authigenic calcites. Symbols as indicated for: (A) Soledad Basin; (B) Rainbow Basin; (C) Death Valley area; (D) Lake Mead area; and (E) western Arizona.

in authigenic calcite  $\delta^{18}\text{O}$  values. Therefore, we suggest the effects of temperature can be ignored in the current discussion, as most of the authigenic mineral isotopic records produced show an overall increase of  $\sim 2\text{--}8\text{‰}$  in  $\delta^{18}\text{O}$  values since the middle Miocene (Fig. 4). Temperature effects alone are not likely to have significantly contributed to the general patterns recognized in the central Basin and Range isotopic records.

### Evaporation Effects

Three lines of evidence suggest that the Neogene surface waters present throughout the central Basin and Range Province were intermittently subject to evaporative modification. First, evaporite minerals are recognized locally in three of the stratigraphic sections investigated. In the Soledad Basin, the Tick Canyon–Volcanic member of the Lower Miocene Vasquez Formation hosts economic borate deposits that are interpreted as forming in a playa lake not unlike the modern floor of Death Valley (Oakeshott, 1965). Similar occurrences of evaporite minerals are found in the Death Valley and Lake Mead area stratigraphic sections (Bohannon, 1984; Wright et al., 1999). Second, the presence of zeolitic ashes in the Rainbow Basin and western Arizona stratigraphic sections suggests the presence of saline surface waters during ash deposition (Sheppard and Gude, 1973; Woodburne et al., 1990). Third, authigenic smectites from the El Paso and Rainbow Basin

stratigraphic sections have  $\delta\text{D}$  and  $\delta^{18}\text{O}$  values that suggest these samples formed in the presence of surface waters modified by evaporation (Fig. 3). Authigenic smectites forming in isotopic equilibrium with surface waters that are not modified by evaporation should plot parallel to the global meteoric water line (Savin and Hsieh, 1998). This parallel trend is recognized in smectites from the western and northern Great Basin (Horton et al., 2004; Fig. 3); however, the smectite samples from the El Paso Basin and Rainbow Basin plot subparallel to the meteoric water line along an evaporative trend (Fig. 3). X-ray diffractograms indicate that all smectites investigated are similar-composition montmorillonites, suggesting the observed interbasinal variation in smectite isotopic composition is not due to differences in the chemical composition of these clays. Fourth, the Sr/Ca ratios of lacustrine carbonates from the Rainbow Basin and Death Valley regions suggest the lake waters present during the time of mineral formation were saline (Fig. 6). Previous research indicates that the Sr/Ca ratios of lacustrine carbonates are good proxy indicators of paleosalinity (Chivas et al., 1993). The Sr/Ca ratios determined for lacustrine carbonates in the Rainbow Basin and Death Valley stratigraphic sections range between 0.0001 and 0.01 (Table 1; Fig. 6); lacustrine carbonate Sr/Ca ratios between 0.001 and 0.01 have been correlated with lacustrine salinities of  $\sim 10\text{‰}$  to  $\sim 100\text{‰}$  (Chivas et al., 1993).

Covariant trends in calcite  $\delta^{13}\text{C}$  and  $\delta^{18}\text{O}$  values provide further evidence for evaporative modification of surface waters during deposition of specific stratigraphic intervals. Isotopic covariance in the limestone Ubehebe Formation (Death Valley area) and the Thumb Member of the Horse Spring Formation (Lake Mead Basin) suggests that deposition of these lithostratigraphic units occurred under persistent closed hydrologic conditions (Talbot, 1990; Fig. 5). Isotopic covariance in lacustrine carbonates is believed to result from coupled outgassing of  $^{12}\text{C}$ -rich  $\text{CO}_2$  and evaporation of  $^{16}\text{O}$ -rich  $\text{H}_2\text{O}$  from closed basin lake surface waters (Talbot and Kelts, 1990). Thus, the strong isotopic covariance in the limestone Ubehebe Formation and the Thumb Member of the Horse Spring Formation suggests that the wide range in calcite  $\delta^{18}\text{O}$  values recognized in these two lithostratigraphic units results from evaporative enrichment of ancient lake waters.

In contrast, the lack of isotopic covariance, characteristic of the majority of the lithostratigraphic units investigated (Fig. 5), does not necessarily indicate the lack of evaporative modification of surface water isotopic compositions under hydrologically open conditions. For example, deposition of the Furnace Creek Formation most certainly occurred under episodic evaporative conditions due to the presence of evaporite mineral layers within this unit. Yet, there is no apparent isotopic covariance in Furnace Creek Formation carbonates (Fig. 5C).

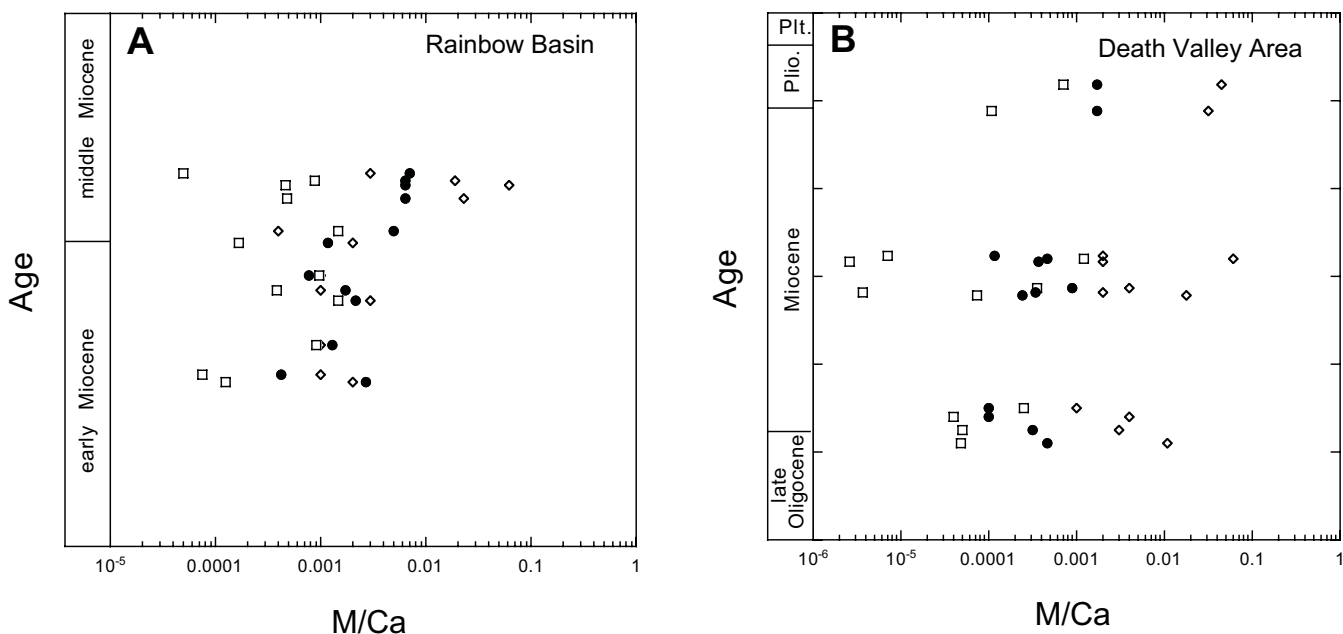


**Figure 6.** Carbonate trace-element ratio records for the Rainbow Basin (A) and Death Valley area (B) stratigraphic sections. Ratios shown are Mg/Ca (diamonds), Sr/Ca (filled circles), and Mn/Ca (squares). M—metal cation; Plio.—Pliocene; Plt.—Pleistocene.

In this example, surface water evaporation is most likely responsible for the highly variable calcite  $\delta^{18}\text{O}$  values recognized in the Furnace Creek Formation ( $\sim -11$  to  $\sim -5\text{‰}$ ), and such highly variable oxygen isotope values have been observed in other ancient lake systems of the Great Basin that are clearly the result of evaporation (Abruzzese et al., 2005).

Despite the fact that there is clear evidence for evaporative modification of surface waters in portions of all the stratigraphic sections investigated, we do not believe evaporation was a significant contributor to the overall pattern recognized in the authigenic mineral isotopic records. Evaporation certainly contributed to the range in authigenic mineral  $\delta^{18}\text{O}$  values recognized within a specific stratigraphic interval characterized by continuous lacustrine sedimentation. However, all of the stratigraphic sections investigated include terrestrial sedimentary rocks of highly variable lithologies, including coarse-grained fluvial facies, which indicate the conditions of deposition in each of the basin systems investigated changed in response to dynamic tectonic, topographic, and climatic conditions. Moreover, we find similar isotopic trends in other lacustrine stratigraphic sections in the Great Basin, and these isotopic trends are not the result of evaporation (Horton et al., 2004).

In summary, we suggest extra-basinal processes, such as regional climate change and regional uplift-downdrop, are the primary mechanisms of the long-term trends ( $>107$  yr) recognized in authigenic mineral stable isotope records, rather than simple evaporative modification of surface waters. Evaporation is a significant contributor to the variability in authigenic mineral  $\delta^{18}\text{O}$  values for specific stratigraphic intervals, but is not responsible for the long-term pattern recognized in the isotopic records.

### Diagenetic Effects

The isotopic compositions of authigenic minerals are sensitive to diagenetic recrystallization (Dickson and Coleman, 1980; Morrill and Koch, 2002; Garzzone et al., 2004). Diagenesis at elevated temperatures and in the presence of crustal fluids may overprint primary surficial carbonate isotopic compositions, thus limiting the utility of carbonate oxygen isotope ratios as paleotopographic proxies. These conditions are characteristic of the burial diagenesis realm, whereas meteoric diagenesis occurs in the near-surface environment in the presence of meteoric-derived ground and pore waters (Tucker and Bathurst, 1990). As such, it is imperative that extent of burial versus meteoric diagenesis, where present, be constrained.

Several lines of evidence suggest that the samples investigated were not affected by burial diagenesis. First, petrographic investigation of prepared thin sections stained with alizarin red S and potassium ferricyanide indicate that low magnesium calcite is the dominant carbonate mineral present in all stratigraphic sections investigated, which suggests that diagenetic overprinting during dolomitization did not occur. Second, sparry calcite, a common product of diagenetic carbonate cementation, was not observed in any of the carbonate samples investigated. Third, all polished thin sections investigated exhibited uniform dull luminescence, suggesting carbonate diagenesis in the presence of  $\text{Mn}^{2+}$ -bearing waters (i.e., reducing waters) did not occur. Fourth, carbonate trace-element compositions further support the interpretation that burial diagenesis did not affect the samples investigated here. Variations in trace-element partitioning in carbonates are a function of mineral precipitation rate, mineral stoichiometry, crystal growth mechanisms, fluid composition, and temperature (Banner, 1995). A detailed discussion of each of these variables is beyond the scope of this investigation; however, the low Mg/Ca and Mn/Ca ratios in 26 calcites investigated from the Rainbow Basin and Death Valley sections suggest diagenetic overprinting of primary, low-magnesium calcite did not occur (Table 1; Fig. 6).

### Paleotopographic and Surface Water Source Region Effects

Based on the arguments presented herein, we suggest the general patterns recognized in the Neogene authigenic mineral stable isotopic records are primarily due to changes in regional surface elevation and surface water source region since the early Miocene. The similarity in the age, magnitude, and rate of change of authigenic mineral  $\delta^{18}\text{O}$  values in the Neogene isotopic records for the Soledad Basin, Rainbow Basin, Death Valley region, and western Arizona oxygen isotope records (Fig. 2) suggests a regional mechanism for the observed isotopic patterns. As presented already, latitude, longitude, temperature, evaporation, and diagenetic effects alone are not likely to be responsible for producing the observed patterns in these isotopic records. A global mechanism is also not likely due to disparities between the Lake Mead Basin isotopic record (this study), similar-age authigenic mineral isotopic records elsewhere in western North America (Kohn et al., 2002; Takeuchi and Larson, 2005; Sjoström et al., 2006), and the Soledad Basin, Rainbow Basin, Death Valley region, and western Arizona oxygen isotope records. We suggest that a regional

mechanism, involving surficial lowering of the central Basin and Range and concomitant channelization of southerly storm tracks, is responsible for the similar patterns recognized in these authigenic mineral isotopic records.

In a strict paleotopographic interpretation of the data, the general pattern of an  $\sim 2\text{‰}$ – $8\text{‰}$  increase in authigenic mineral  $\delta^{18}\text{O}$  values during the Miocene requires  $\sim 1$ – $3$  km of surface elevation decrease. Given the spatial distribution of the stratigraphic sections investigated, this topographic lowering would be best explained by downdrop of a regional plateau, rather than collapse of a specific orographic barrier. The case for regional subsidence agrees well with the tectonic evolution of the region.

All of the terrestrial sedimentary sequences investigated were deposited in accommodation space provided by extensional tectonics. Thermochronologic data from the California Transverse Ranges suggest that Miocene cooling events in the San Gabriel and San Bernardino Mountains correlate with extensional exhumation of the ranges (Blythe et al., 2000). This interpretation is consistent with sedimentologic investigations in the adjacent Soledad Basin, which suggest the basin formed in response to crustal extension/rifting since the latest Oligocene (e.g., Hendrix and Ingersoll, 1987). Similarly, sedimentologic investigations suggest an early-middle Miocene extensional origin for the Rainbow Basin (Ingersoll et al., 1996), and the extensional nature of basin formation in the Death Valley region is well known (Cemen et al., 1999; Snow and Lux, 1999; Wright et al., 1999). Miocene terrestrial sedimentation in western Arizona is also believed to be associated with extensional tectonics in the Colorado River Extensional Corridor (Spencer et al., 1989).

Based on the authigenic mineral isotopic records presented here, we suggest that crustal extension contributed to a net elevation decrease throughout the region. The observed Neogene shift in authigenic mineral oxygen isotope ratios agrees well with the timing of crustal extension across the central Basin and Range (Anderson, 1971). Previous geophysical and structural arguments have suggested that the large amounts of Neogene crustal extension in the central Basin and Range may be responsible for the  $\sim 1$  km topographic step recognized between the northern Great Basin and Las Vegas regions (Wernicke et al., 1988). Furthermore, sediment dispersal patterns in the Death Valley region indicate a change from closed basin sediment accumulation to south-directed fluvial transport of sediment during the middle Miocene (Snow and Lux, 1999; Snow and Wernicke, 2000). This shift in paleohydrology agrees well with a south-directed

topographic lowering of the central Basin and Range during Neogene extension.

However, authigenic mineral isotopic compositions are also sensitive to changes in the isotopic composition of ancient surface waters due to changes in water source region. Changes in surface water source region occur in two main ways. First, reorganization of regional climate patterns, in response to regional topographic change or alteration of oceanic circulation patterns, may cause a shift in the isotopic composition of precipitation, and thus, surface waters. Second, reorganization of the drainage systems feeding into lake basins may cause a shift in the isotopic composition of local surface waters.

With respect to the regional climate patterns, a multiyear study conducted in the central Basin and Range Province indicates that winter precipitation, derived from dominantly westerly storm tracks, is on average  $\sim 5\%$  lower in  $\delta^{18}\text{O}$  value than summer precipitation, derived from dominantly southerly storm tracks throughout the region (Table 8 of Friedman et al., 1992). At present, more than half of the total annual precipitation reaching both the central and northern Basin and Range Province follows a southerly storm track (Friedman et al., 2002a). Friedman et al. (1992) suggested that the difference in isotopic composition of westerly versus southerly precipitation sources is primarily due to differences in the elevation of the topographic barriers intersected by the two storm tracks. Based on these considerations, we suggest that the regional patterns recognized in the Neogene central Basin and Range isotopic records may have been caused by a prolonged reorganization of regional climate patterns, from a dominantly westerly source to a more southerly source during the Miocene. The reorganization of climate patterns does not conflict with our previous suggestion of extension-driven elevation decrease during the Miocene throughout the central Basin and Range. Rather, the two processes agree well in that it is not difficult to envision channeling of air masses into the topographic low created by east-west extension of the central Basin and Range since the early Miocene.

In contrast to the isotopic shifts recognized in the Soledad Basin, Rainbow Basin, Death Valley region, and western Arizona records, the El Paso Basin record of Poage and Chamberlain (2002) shows a more rapid increase in  $\delta^{18}\text{O}$  values between the middle and late Miocene. As described already, the El Paso Basin authigenic mineral  $\delta^{18}\text{O}$  values are also anomalous in that they are generally lower than  $\delta^{18}\text{O}$  values from similar-age sediments from the northern and western Great Basin and generally higher than the more proximal central Basin and Range values. Clearly, a local mechanism is responsible

for the disparities between the El Paso Basin record and the records produced in the current investigation.

The proximity of the El Paso Basin to the southern Sierra Nevada allows for the possibility that precipitation and surface waters derived from both higher elevation (Sierran) sources and lower elevation (Mojave) sources fed into the basin during its development. Following this logic, the El Paso Basin isotopic record suggests middle Miocene (ca. 14 Ma) surface waters in the El Paso Basin were derived from a westerly precipitation source that intersected the high Sierra Nevada, whereas late Miocene (ca. 7 Ma) surface waters feeding into the El Paso Basin were derived from a southerly precipitation source. Sedimentologic studies of the Miocene El Paso Basin stratigraphy indicate the Sierra Nevada became a sediment source area for the El Paso Basin at ca. 8 Ma (Loomis and Burbank, 1988). This change in sediment provenance could be explained by topographic lowering of the El Paso Basin, relative to the crest of the range, which is in good agreement with the El Paso Basin authigenic mineral isotopic record. Topographic lowering of the El Paso Basin along the Sierra Nevada Range Front fault during the middle to late Miocene, and resultant exposure to the developing southerly storm track described in the previous paragraphs, offers an explanation for the anomalous characteristics of the El Paso Basin isotopic record.

The Miocene authigenic calcite stable isotopic record from the Lake Mead area differs from all of the other records presented in that it exhibits an  $\sim 5\%$  decrease in calcite  $\delta^{18}\text{O}$  values during the early Miocene, recognized within the Horse Spring Formation (Fig. 2D). The Horse Spring Formation is significant because the lowermost Rainbow Gardens Member represents the only pre-extensional sedimentary rocks investigated in the current study, and deposition of the Horse Spring Formation is contemporaneous with large-volume, mantle-derived magmatism in the region (Beard, 1996). Paleogeographic reconstruction of the Lake Mead Basin suggests that uplift of the now-adjacent Virgin Mountains occurred during deposition of the Horse Spring Formation (Beard, 1996). We believe the Lake Mead Basin oxygen isotope record provides further evidence of surficial uplift during the Miocene. The  $\sim 5\%$  decrease in calcite  $\delta^{18}\text{O}$  values recognized in the Horse Spring Formation indicates up to 1.5 km of surface uplift in the Lake Mead region may have occurred during deposition of the Miocene Horse Spring Formation, contemporaneous with local magmatic activity. This interpretation is in good agreement with the recent correlation between regional magmatism and surface uplift in the northern Basin and

Range Province during the Eocene (Horton et al., 2004).

## CONCLUSIONS

The authigenic mineral stable isotopic records presented here provide evidence for the topographic response of the central Basin and Range Province to regional Neogene crustal dynamics. The  $\delta^{18}\text{O}$  records for the Rainbow Basin, El Paso Basin, Death Valley region, and western Arizona stratigraphic sections provide no evidence for surficial uplift in the region, but rather indicate that the central Basin and Range Province experienced a net topographic lowering during the Neogene causing a reorganization of regional atmospheric circulation patterns from a westerly dominated to southerly dominated precipitation source. This regional surface subsidence is contemporaneous with extensional deformation of the crust, suggesting a link between extension and elevation decrease in the Basin and Range Province. As such, our data reinforce models of the central Basin and Range Province that call for extensional collapse and topographic subsidence of a previously uplifted plateau (Jones et al., 1998; Sonder and Jones, 1999).

The authigenic calcite  $\delta^{18}\text{O}$  record for the Lake Mead Basin supports previous sedimentologic arguments for Miocene surface uplift in the area (Beard, 1996). The timing of surface uplift, between the early and late Miocene, is similar to the timing of magmatic activity in the Lake Mead area (Beard, 1996). This relationship between magmatic activity and surface uplift has also been observed in the northern Great Basin (Horton et al., 2004), although in the northern Great Basin, surface uplift occurred earlier, between Eocene and Oligocene epochs. We suggest that surface uplift and magmatic activity are intimately linked in the Great Basin, such that surface uplift sweeps southward in time coincident with the southern migration of magmatism (Armstrong and Ward, 1991). This spatial and temporal variation of surface uplift and magmatism supports models that tie mantle-derived magmatism with surface uplift of western North America (Platt and England, 1993; Humphreys, 1995; Sonder and Jones, 1999).

## ACKNOWLEDGMENTS

Support for this research was provided by National Science Foundation (NSF) grants EAR-0309011 and EAR-0217128 to Chamberlain, and a GSA student research grant and a Stanford University School of Earth Sciences McGee grant to Horton. Special thanks are due to the National Park Service for granting us research permit DEVA-2003-SCI-0033 for sample collection in Death Valley National Park. Constructive reviews by I. Montanez, B. Wernicke, and Y. Dilek improved the original manuscript.

## REFERENCES CITED

- Abruzzese, M.J., Waldbauer, J.R., and Chamberlain, C.P., 2005, Oxygen and hydrogen isotope ratios of fresh-water chert as indicators of ancient climate and hydrologic regime: *Geochimica et Cosmochimica Acta*, v. 69, p. 1377–1390.
- Anderson, R.E., 1971, Thin-skin distension in Tertiary rocks of southwestern Nevada: *Geological Society of America Bulletin*, v. 82, p. 43–58.
- Anderson, R.E., Longwell, C., Armstrong, R., and Marvin, R., 1972, Significance of K-Ar ages of Tertiary rocks from the Lake Mead region, Nevada-Arizona: *Geological Society of America Bulletin*, v. 83, p. 273–288.
- Armstrong, R.L., and Ward, P., 1991, Evolving geographic patterns of Cenozoic magmatism in the North American Cordillera: The temporal and spatial association of magmatism and metamorphic core complexes: *Journal of Geophysical Research*, v. 96, p. 13,201–13,224.
- Axelrod, D.I., 1962, Post-Pliocene uplift of the Sierra Nevada of California: *Geological Society of America Bulletin*, v. 73, p. 183–198.
- Banner, J.L., 1995, Application of the trace element and isotope geochemistry of strontium to studies of carbonate diagenesis: *Sedimentology*, v. 42, p. 805–824.
- Beard, L.S., 1996, Paleogeography of the Horse Spring Formation in relation to the Lake Mead fault system, Virgin Mountains, Nevada and Arizona in *Beratan, K.K., ed., Reconstructing the history of Basin and Range extension using sedimentology and stratigraphy: Geological Society of America Special Paper 303*, p. 27–60.
- Blair, T.C., and Reynolds, R.G., 1999, Sedimentology and tectonic implications of the Neogene synrift Hole in the Wall and Wall Front Members, Furnace Creek basin, Death Valley, California, in *Wright, L.A., and Troxel, B.W., eds., Cenozoic basins of the Death Valley region: Geological Society of America Special Paper 333*, p. 127–168.
- Blythe, A.E., Burbank, D.W., Farley, K.A., and Fielding, E.J., 2000, Structural and topographic evolution of the central Transverse Ranges, California, from apatite fission-track, (U-Th)/He and digital elevation model analyses: *Basin Research*, v. 12, p. 97–114, doi: 10.1046/j.1365-2117.2000.00116.x.
- Bohannon, R.G., 1984, Nonmarine sedimentary rocks of Tertiary age in the Lake Mead region, southeastern Nevada and northwestern Arizona: U.S. Geological Survey Professional Paper 1259, 72 p.
- Cemen, I., Wright, L.A., and Prave, A.R., 1999, Stratigraphy and tectonic implications of the latest Oligocene and early Miocene sedimentary succession, southernmost Mineral Mountains, Death Valley region, California, in *Wright, L.A., and Troxel, B.W., eds., Cenozoic basins of the Death Valley region: Geological Society of America Special Paper 333*, p. 65–86.
- Chamberlain, C.P., and Poage, M.A., 2000, Reconstructing the paleotopography of mountain belts from the isotopic composition of authigenic minerals: *Geology*, v. 28, p. 115–118, doi: 10.1130/0091-7613(2000)028<0115:RTPOMB>2.3.CO;2.
- Chamberlain, C.P., Poage, M.A., Craw, D., and Reynolds, R.C., 1999, Topographic development of the Southern Alps recorded by the isotopic composition of authigenic minerals, South Island, New Zealand: *Chemical Geology*, v. 155, p. 279–294, doi: 10.1016/S0009-2541(98)00165-X.
- Chivas, A.R., De Decker, P., Cali, J.A., Chapman, A., Kiss, E., and Shelley, J.M.G., 1993, Coupled stable-isotope and trace-element measurements of lacustrine carbonates as paleoclimatic indicators, in *Swart, P.K., Lohmann, K.C., McKenzie, J.A., and Savin, S., eds., Climate change in continental isotopic records: American Geophysical Union Geophysical Monograph 78*, p. 113–121.
- Christensen, M.N., 1966, Late Cenozoic crustal movements in the Sierra Nevada of California: *Geological Society of America Bulletin*, v. 77, p. 163–182.
- Clayton, R.N., and Mayeda, T.K., 1963, The use of bromine pentafluoride in the extraction of oxygen from oxides and silicates for isotopic analysis: *Geochimica et Cosmochimica Acta*, v. 27, p. 43–52, doi: 10.1016/0016-7037(63)90071-1.
- Craig, H., 1961, Isotopic variations in meteoric waters: *Science*, v. 133, p. 1702–1703.
- Criss, R.N., 1999, Principles of stable isotope distribution: New York, Oxford University Press, 254 p.
- Crowell, J.C., 1973, Problems concerning the San Andreas fault system in southern California, in *Kovach, R.L., and Nur, A., eds., Conference on Tectonic Problems of the San Andreas Fault System, Proceedings: Stanford University Publications in the Geological Sciences*, v. 13, p. 125–135.
- Dansgaard, W., 1964, Stable isotopes in precipitation: *Tellus*, v. 16, p. 436–468.
- Dettman, D.L., Fang, X., Garzzone, C.N., and Li, J., 2003, Uplift-driven climate change at 12 Ma: A long  $\delta^{18}\text{O}$  record from the NE margin of the Tibetan Plateau: *Earth and Planetary Science Letters*, v. 6764, p. 1–11.
- Dickson, J.A.D., and Coleman, M.L., 1980, Changes in carbon and oxygen isotopic composition during limestone diagenesis: *Sedimentology*, v. 27, p. 107–118.
- Ducea, M., and Saleeby, J., 1998, A case for delamination of the deep batholithic crust beneath the Sierra Nevada, California: *International Geology Review*, v. 40, p. 78–93.
- Durham, J.W., Jahns, R.H., and Savage, D.E., 1954, Marine-nonmarine relationships in the Cenozoic section of California: California Division of Mines Bulletin, v. 170, p. 59–72.
- Ehler, K.W., 1982, Basin analysis of the Miocene Mint Canyon Formation, southern California, in *Ingersoll, R.V., and Woodburne, M.O., eds., Cenozoic deposits of California and Arizona: Los Angeles, Pacific Section, Society of Economic Paleontologists and Mineralogists*, 112 p.
- Farmer, G.L., Glazner, A.F., and Manley, C.R., 2002, Did lithospheric delamination trigger late Cenozoic potassic volcanism in the southern Sierra Nevada, California?: *Geological Society of America Bulletin*, v. 114, p. 754–768, doi: 10.1130/0016-7606(2002)114<0754:DLDTLC>2.0.CO;2.
- Fliedner, M.M., and Ruppert, S., 1996, Three-dimensional crustal structure of the southern Sierra Nevada from seismic fan profiles and gravity modeling: *Geology*, v. 24, p. 367–370, doi: 10.1130/0091-7613(1996)024<0367:TDCSOT>2.3.CO;2.
- Friedman, I., Smith, G.I., Gleason, J.D., Warden, A., and Harris, J.M., 1992, Stable isotope composition of waters in southeastern California. 1. Modern precipitation: *Journal of Geophysical Research*, v. 97, p. 5795–5812.
- Friedman, I., Harris, J.M., Smith, G.I., and Johnson, C.A., 2002a, Stable isotope composition of waters in the Great Basin, United States. 1. Air-mass trajectories: *Journal of Geophysical Research*, v. 107, p. 14–14-14.
- Friedman, I., Smith, G.I., Johnson, C.A., and Moscati, R.J., 2002b, Stable isotope composition of water in the Great Basin, United States. 2. Modern precipitation: *Journal of Geophysical Research*, v. 107, p. 15–15-22.
- Garzzone, C.N., Dettman, D.L., Quade, J., DeCelles, P.G., and Butler, R.F., 2000, High times on the Tibetan Plateau: Paleoelevation of the Thakkhola graben, Nepal: *Geology*, v. 28, p. 339–342, doi: 10.1130/0091-7613(2000)028<0339:HTOTTP>2.3.CO;2.
- Garzzone, C.N., Dettman, D.L., and Horton, B.K., 2004, Carbonate oxygen isotope paleoaltimetry: Evaluating the effect of diagenesis on paleoelevation estimates for the Tibetan Plateau: *Paleogeography, Palaeoclimatology, Palaeoecology*, v. 212, p. 119–140, doi: 10.1016/j.palaeo.2004.05.020.
- Hendrix, E.D., and Ingersoll, R.V., 1987, Tectonics and alluvial sedimentation of the upper Oligocene/lower Miocene Vasquez Formation, Soledad Basin, southern California: *Geological Society of America Bulletin*, v. 98, p. 647–663, doi: 10.1130/0016-7606(1987)98<647:TAASOT>2.0.CO;2.
- Horton, T.W., Sjöström, D.J., Abruzzese, M.J., Poage, M.A., Waldbauer, J.R., Hren, M., Wooden, J., and Chamberlain, C.P., 2004, Spatial and temporal variation of Cenozoic surface elevation in the Great Basin and Sierra Nevada: *American Journal of Science*, v. 304, p. 862–888.
- House, M.A., Wernicke, B.P., and Farley, K.A., 1998, Dating topography of the Sierra Nevada, California, using apatite U-Th/He ages: *Nature*, v. 396, p. 66–69, doi: 10.1038/23926.
- Huber, N.K., 1981, Amount and timing of late Cenozoic uplift and tilt of the central Sierra Nevada, California—Evidence from the upper San Joaquin River basin: U.S. Geological Survey Professional Paper 1197, Report P, 28 p.
- Humphreys, E.D., 1995, Post-Laramide removal of the Farallon slab, western United States: *Geology*, v. 23, p. 987–990, doi: 10.1130/0091-7613(1995)023<0987:PLROTF>2.3.CO;2.
- Ingersoll, R.V., Devaney, K.A., Geslin, J.K., Cavazza, W., Diamond, D.S., Heins, W.A., Jagiello, K.J., Marsaglia, K.M., Paylor, E.D., and Short, P.F., 1996, The Mud Hills, Mojave Desert, California: Structure, stratigraphy, and sedimentology of a rapidly extended terrane, in *Beratan, K.K., ed., Reconstructing the history of Basin and Range extension using sedimentology and stratigraphy: Geological Society of America Special Paper 303*, p. 61–84.
- Jones, C.H., Sonder, L.J., and Unruh, J.R., 1998, Lithospheric gravitational potential energy and past orogenesis: implications for conditions of initial Basin and Range and Laramide deformation: *Geology*, v. 26, p. 639–642, doi: 10.1130/0091-7613(1998)026<0639:LGPEAP>2.3.CO;2.
- Jones, C.H., Farmer, G.L., and Unruh, J., 2004, Tectonics of Pliocene removal of lithosphere of the Sierra Nevada, California: *Geological Society of America Bulletin*, v. 116, p. 1408–1422, doi: 10.1130/B25397.1.
- Kim, S., and O'Neil, J.R., 1997, Equilibrium and nonequilibrium oxygen isotope effects in synthetic carbonates: *Geochimica et Cosmochimica Acta*, v. 61, p. 3461–3475, doi: 10.1016/S0016-7037(97)00169-5.
- Kohn, M.J., Miselis, J.L., and Fremd, T.J., 2002, Oxygen isotope evidence for progressive uplift of the Cascade Range, Oregon: *Earth and Planetary Science Letters*, v. 204, p. 151–165, doi: 10.1016/S0012-821X(02)00961-5.
- Loomis, D.P., and Burbank, D.W., 1988, The stratigraphic evolution of the El Paso Basin, southern California: Implications for the Miocene development of the Garlock fault and uplift of the Sierra Nevada: *Geological Society of America Bulletin*, v. 100, p. 12–28, doi: 10.1130/0016-7606(1988)100<0012:TSEOTE>2.3.CO;2.
- MacFadden, B.J., Swisher, C.C., Opydyke, N.D., and Woodburne, M.O., 1990, Paleomagnetism, geochronology, and possible tectonic rotation of the middle Miocene Barstow Formation, Mojave Desert, southern California: *Geological Society of America Bulletin*, v. 102, p. 478–493, doi: 10.1130/0016-7606(1990)102<0478:PGATPR>2.3.CO;2.
- McCrea, J.M., 1950, On the isotopic chemistry of carbonates and a paleotemperature scale: *The Journal of Chemical Physics*, v. 18, p. 849–857, doi: 10.1063/1.1747785.
- Meibom, A., Stage, M., Wooden, J., Constantz, B.R., Dunbar, R.B., Owen, A., Grumet, N., Bacon, C.R., and Chamberlain, C.P., 2003, Monthly strontium/calcium oscillations in symbiotic coral aragonite: Biological effects limiting the precision of the paleotemperature proxy: *Geophysical Research Letters*, v. 30, p. 71–71-4.
- Moore, D.M., and Reynolds, R.C., 1997, X-ray diffraction and the identification and analysis of clay minerals: New York, Oxford University Press, 378 p.
- Morrill, C., and Koch, P.L., 2002, Elevation or alteration? Evaluation of isotopic constraints on paleoaltitudes surrounding the Eocene Green River Basin: *Geology*, v. 30, p. 151–154, doi: 10.1130/0091-7613(2002)030<0151:EOAEOI>2.0.CO;2.
- Morrison, R.R., 1965, Summary of the geology of the Sand Canyon–Placerita Canyon area, in *Placerita-Soledad-Vasquez Rocks area, Soledad Basin, Los Angeles County, California: American Association of Petroleum Geologists Pacific Coast Section Field Trip Guide Book*, 4 p.
- Muehlberger, W.R., 1958, Geology of northern Soledad Basin, Los Angeles County, California: *Bulletin of the American Association of Petroleum Geologists*, v. 42, p. 1812–1844.
- Nagy, E.A., and Murray, B., 1996, Plio-Pleistocene deposits adjacent to the Manix fault: Implications for the history of the Mojave River and Transverse Ranges uplift: *Sedimentary Geology*, v. 103, p. 9–21, doi: 10.1016/0037-0738(95)00076-3.

- Nations, J.D., Landye, J.J., and Hevly, R.H., 1982, Location and chronology of Tertiary sedimentary deposits in Arizona; a review, *in* Ingersoll, R.V., and Woodburne, M.O., eds., Cenozoic nonmarine deposits of California and Arizona: Los Angeles, California, Society of Economic Paleontologists and Mineralogists, p. 107–122.
- Oakeshott, G.B., 1965, Vasquez Formation: American Association of Petroleum Geologists Field Trip Guide Book, 6 p.
- Platt, J.P., and England, P.C., 1993, Convective removal of lithosphere beneath mountain belts: Thermal and mechanical consequences: *American Journal of Science*, v. 293, p. 307–336.
- Poage, M.A., and Chamberlain, C.P., 2001, Empirical relationships between elevation and the stable isotope composition of precipitation and surface waters: Considerations for studies of paleoelevation change: *American Journal of Science*, v. 301, p. 1–15.
- Poage, M.A., and Chamberlain, C.P., 2002, Stable isotopic evidence for a pre–Middle Miocene rain shadow in the western Basin and Range: Implications for the paleotopography of the Sierra Nevada: *Tectonics*, v. 21, p. 1034–1043, doi: 10.1029/2001TC001303.
- Poulson, S.R., and John, B.E., 2003, Stable isotope and trace element geochemistry of the basal Bouse Formation carbonate, southwestern United States: Implications for the Pliocene uplift history of the Colorado Plateau: *Geological Society of America Bulletin*, v. 115, p. 434–444, doi: 10.1130/0016-7606(2003)115<0434:SIATEG>2.0.CO;2.
- Rowley, D.B., Pierrehumbert, R.T., and Currie, B.S., 2001, A new approach to stable isotope-based paleoaltimetry and paleohypsometry of the high Himalaya since the Miocene: *Earth and Planetary Science Letters*, v. 188, p. 253–268, doi: 10.1016/S0012-821X(01)00324-7.
- Rozanski, K., Aragus-Araguas, L., and Gonfiantini, R., 1993, Isotopic patterns in modern global precipitation, *in* Swart, P.K., Lohmann, K.C., McKenzie, J.A., and Savin, S., eds., Climate change in continental isotopic records: American Geophysical Union Geophysical Monograph 78, p. 1–36.
- Rudnick, R.L., and Lee, C., 2002, Osmium isotope constraints on tectonic evolution of the lithosphere in the southwestern United States: *International Geology Review*, v. 44, p. 501–511.
- Ruppert, S., Fliedner, M.M., and Zandt, G., 1998, Thin crust and active upper mantle beneath the southern Sierra Nevada in the western United States: *Tectonophysics*, v. 286, p. 237–252, doi: 10.1016/S0040-1951(97)00268-0.
- Savin, S.M., and Hsieh, J.C.C., 1998, The hydrogen and oxygen isotope geochemistry of pedogenic clay minerals: Principles and theoretical background: *Geoderma*, v. 82, p. 227–253, doi: 10.1016/S0016-7061(97)00103-1.
- Shafiqullah, M., Damon, P.E., Lynch, D.J., Reynolds, S.J., Rehrig, W.A., and Raymond, R.H., 1980, K/Ar geochronology and geologic history of southwestern Arizona and adjacent area: *Arizona Geological Society Digest*, v. 12, p. 210–260.
- Sharp, Z.D., Atudoei, V., and Durakiewicz, T., 2001, A rapid method for determination of hydrogen and oxygen isotope ratios from water and hydrous minerals: *Chemical Geology*, v. 178, p. 197–210, doi: 10.1016/S0009-2541(01)00262-5.
- Sheppard, R.A., and Gude, A.J., III, 1973, Zeolites and associated authigenic silicate minerals in tuffaceous rocks of the Big Sandy Formation, Mohave County, Arizona: U.S. Geological Survey Professional Paper 830, 36 p.
- Sheppard, S.M.F., and Gilg, H.A., 1996, Stable isotope geochemistry of clay minerals: *Clay Minerals*, v. 31, p. 1–24.
- Sjostrom, D.J., Hren, M.T., Horton, T.W., Waldbauer, J.R., and Chamberlain, C.P., 2006, Stable isotopic evidence for an early Tertiary elevation gradient in the Great Plains–Rocky Mountain region, *in* Willet, S., Hovius, N., Fisher, D., and Brandon, M., eds., Tectonics, climate, and landscape evolution: *Geological Society of America Special Paper* 398.
- Smith, A.G., Hurlley, A.M., and Briden, J.C., 1981, Phanerozoic paleocontinental world maps: New York, Cambridge University Press, 102 p.
- Snow, J.K., and Lux, D.R., 1999, Tectono-sequence stratigraphy of Tertiary rocks in the Cottonwood Mountains and northern Death Valley area, California and Nevada, *in* Wright, L.A., and Troxel, B.W., eds., Cenozoic basins of the Death Valley region: *Geological Society of America Special Paper* 333, p. 17–64.
- Snow, J.K., and Wernicke, B., 2000, Cenozoic tectonism in the central Basin and Range; magnitude, rate, and distribution of upper crustal strain: *American Journal of Science*, v. 300, p. 659–719.
- Sonder, L.J., and Jones, C.H., 1999, Western United States extension: How the West was widened: *Annual Reviews of Earth and Planetary Sciences*, v. 27, p. 417–462, doi: 10.1146/annurev.earth.27.1.417.
- Spencer, J.E., Grubensky, M.J., Duncan, J.T., Shenk, J.D., Yarnold, J.C., and Lombard, J.P., 1989, Geology and mineral deposits of the central Artillery Mountains, *in* Spencer, J.E., and Reynolds, S.J., eds., Geology and mineral resources of the Buckskin and Rawhide Mountains, west-central Arizona: *Arizona Geological Society Bulletin*, v. 198, p. 168–183.
- Takeuchi, A., and Larson, P.B., 2005, Oxygen isotope evidence for late Miocene development of an orographic rain shadow in eastern Washington, USA: *Geology*, v. 33, p. 313–316, doi: 10.1130/G21335.1.
- Talbot, M.R., 1990, A review of the paleohydrological interpretation of carbon and oxygen isotopic ratios in primary lacustrine carbonates: *Chemical Geology*, v. 80, p. 261–279.
- Talbot, M.R., and Kelts, K., 1990, Paleolimnological signatures from carbon and oxygen isotopic ratios in carbonates from organic carbon-rich lacustrine sediments, *in* Katz, B.J., ed., Lacustrine basin exploration: case studies and modern analogs: American Association of Petroleum Geologists Memoir 50, p. 99–112.
- Tucker, M.E., and Bathurst, R.G.C., 1990, Carbonate diagenesis: Cambridge, Massachusetts, Blackwell Scientific Publications, Inc., 312 p.
- Wernicke, B., Axen, G.J., and Snow, J.K., 1988, Basin and Range extensional tectonics at the latitude of Las Vegas, Nevada: *Geological Society of America Bulletin*, v. 100, p. 1738–1757, doi: 10.1130/0016-7606(1988)100<1738:BARETA>2.3.CO;2.
- Wernicke, B., Clayton, R., Ducea, M., Jones, C.H., Park, S., Ruppert, S., Saleeby, J., Kent-Snow, K., Squires, L., Fliedner, M., Jiracek, G., Keller, R., Klemperer, S., Luetgert, J., Malin, P., Miller, K., Mooney, W., Oliver, H., and Phinney, R., 1996, Origin of high mountains in the continents: The southern Sierra Nevada: *Science*, v. 271, p. 190–193.
- Wolfe, J.A., Schorn, H.E., Forest, C.E., and Molnar, P., 1997, Paleobotanical evidence for high altitudes in Nevada during the Miocene: *Science*, v. 276, p. 1672–1675, doi: 10.1126/science.276.5319.1672.
- Woodburne, M.O., Tedford, R.H., and Swisher, C.C., 1990, Lithostratigraphy, biostratigraphy, and geochronology of the Barstow Formation, Mojave Desert, southern California: *Geological Society of America Bulletin*, v. 102, p. 459–477, doi: 10.1130/0016-7606(1990)102<0459:LBAGOT>2.3.CO;2.
- Wright, L.A., Greene, R.C., Cemen, I., Johnson, F.C., and Prave, A.R., 1999, Tectonostratigraphic development of the Miocene–Pliocene Furnace Creek basin and related features, Death Valley region, California, *in* Wright, L.A., and Troxel, B.W., eds., Cenozoic basins of the Death Valley region: *Geological Society of America Special Paper* 333, p. 87–114.
- Zachos, J., Pagani, M., Sloan, L., Thomas, E., and Billups, K., 2001, Trends, rhythms, and aberrations in global climate 65 Ma to present: *Science*, v. 292, p. 686–692, doi: 10.1126/science.1059412.

MANUSCRIPT RECEIVED BY THE SOCIETY 13 FEBRUARY 2005  
 REVISED MANUSCRIPT RECEIVED 15 AUGUST 2005  
 MANUSCRIPT ACCEPTED 19 AUGUST 2005

Printed in the USA